AN EXPERIMENTAL AND THEORETICAL STUDY OF THE NON-EQUILIBRUIM PLASMA IN THERMIONIC DISCHARGES

Ronald H Curry, et al

Sperry Rand Research Center
Sudbury, Massachusetts

January 1968

AN EXPERIMENTAL AND THEORETICAL STUDY OF THE NON-EQUILIBRIUM PLASMA IN THERMIONIC DISCHARGES

by

R. H. Curry, D. W. Norcross, P. M. Stone and K. J. Nygaard

Sperry Rand Research Center

FINAL REPORT

JANUARY 1968

Contract No. Nonr 5154(00)

Prepared for
OFFICE OF NAVAL RESEARCH
WASHINGTON, D. C.

SPERRY RAND RESEARCH CENTER
SUDBURY, MASSACHUSETTS 01776

68

SRRC–CR–68–4
JANUARY 1968

AN EXPERIMENTAL AND THEORETICAL STUDY OF THE NON-EQUILIBRIUM PLASMA IN THERMIONIC DISCHARGES

by

R. H. Curry,* D. W. Norcross,† P. M. Stone** and K. J. Nygaard

Sperry Rand Research Center

FINAL REPORT

Contract No. Nonr 5154(00)

* Present Address: Jarrell-Ash Co.
590 Lincoln St.
Waltham, Mass.

† Present Address: Dept. of Physics
University College London
Gower St.
London W. C. 1
England

** Present Address: Dept. of Physics
Univ. of Pittsburg
Pittsburg, Pa. 15215

SPERRY RAND RESEARCH CENTER
SUDBURY, MASSACHUSETTS 01776

ABSTRACT

This report includes a theoretical discussion of energy loss rates and transport equations in thermionic converters, as well as spectroscopic measurements on a cesium diode and a determination of the electron impact ionization cross-section in cesium.

Theoretically, effective coefficients for ionization and radiative energy loss have been computed for different values of electron temperature and density. These coefficients and the neutral density yield the rates for net ion production and radiative energy loss from all sources except the resonance lines. Energy loss from resonance lines and the ion production cost are considered separately. The following general conclusions can be drawn from the consistent behavior of the results: (1) the area within 0.4 mm of the emitter is a source of ion-electron pairs, the rest of the plasma being a sink; (2) inelastic energy losses decrease monotonically from the emitter to the collector; and (3) these effects are relatively independent of cesium pressure, but are generally proportional to output current density.

Furthermore, the differential equations governing the transport of particles, momentum, and energy in the plasma between the electrodes of a thermionic converter have been formulated in a more complete fashion than has been done previously. Specific advances are the inclusion of more exact coefficients for electron transport and for ion production and radiative energy loss in the plasma volume.

In the diode experiments, the electron temperature T_e was determined from measurement of the continuum emitted by radiative recombination to the 6P states of cesium, and the electron density N_e was determined from Stark broadening of the fundamental series lines. By transversing the monochromator with respect to the discharge, spatial measurements of N_e and T_e were made. Of particular interest is observation of forbidden lines. The 7269 Å line ($6G - 5D_{5/2}$) has a very definite structure in the middle and sharp fall-offs in the wings; its shape depends strongly on electron density.

The total ionization due to the passage of an electron beam in cesium vapor has been measured with a Tate and Smith-type apparatus. The retarding potential difference method was used in the electron gun to obtain energy resolution better than 0.1 eV. The density of Cs atoms was determined from the Taylor and Langmuir tables and also measured with a surface ionization detector. The two methods give the same density to within $\pm$ 3% when the apparatus is in thermodynamic equilibrium with the Cs reservoir. The cross section for production of Cs^+ ions has been determined from threshold to 100 eV. For energies above 50 eV the results agree closely with those of McFarland and Kinney.[2] At threshold we found a slope of 2.7 $Å^2$/eV, as compared to the value 2.2 $Å^2$/eV determined by Heil and Scott.

TABLE OF CONTENTS

LIST OF ILLUSTRATIONS

1.0 INTRODUCTION

This is the Second Annual and also the Final Report on Contract Nonr 5154(00), covering the period from 1 November 1966 to 31 October 1967. The objective of the work performed under this contract has been to determine the properties of the cesium plasma in the ignited (or arc) mode of operation of a thermionic converter.

The experimental part of the program has involved spectroscopic measurements to determine electron temperatures and densities in the inter-electrode plasma of a converter and to explore features of the spectrum for use in refined diagnostic techniques. Ionization cross sections have also been measured in a separate experiment, with particular attention on the threshold region. Theoretical work has developed transport equations that properly account for interaction between the three components (ions, electrons and neutral atoms) of the cesium plasma. These equations allow the prediction of variations of electron density and temperature when initial conditions are given.

The present work has contributed to the growing knowledge of plasma behavior in converters. The use of spectroscopy in thermionics research, initiated at Los Alamos, has been a major factor in achieving our present understanding. There is still much to be done to refine spectroscopic techniques. Forbidden-line intensities offer further information about plasma conditions and have not yet been utilized. The data on forbidden lines presented in this report are the first quantitative results that we know of for cesium.

Transport of electrons, energy, and momentum across the plasma is fundamental to converter operation. Inelastic and elastic rates for energy exchange between electrons, neutrals and ions are now quantitative enough to attempt solution of the relevant equations. This program has contributed to our knowledge of these rates, and in this report the transport equations have been formulated for computer solution.

Satisfactory understanding of plasma effects in thermionics is the practical goal of much continuing research. Towards that goal this work has been dedicated.

2.0 THEORY

The theoretical program has been directed toward describing the transport of particles and energy across the plasma. This is a part of the more general problem of predicting current-voltage characteristics of a diode.

The first year's program defined a model for the interaction of the ions, electrons, and atoms in the plasma and determined effective ionization and recombination rates. The present (second) year's program has gone considerably further. Rates for energy loss of the electrons have been calculated and the equations for transport of particles, momentum, and energy have been formulated for typical "high density" ($N_e \simeq 10^{14} cm^{-3}$) diode conditions. A rather complete description of the plasma in the high density diode is now available.

2.1 Electron Kinetic Energy Loss Rates

Consider a steady state plasma at a given electron density, electron temperature, and total pressure. This is the proper description of the plasma in a thermionic diode, although the temperature and density vary across the interelectrode space. The plasma is optically thin to radiative decay from upper levels, except for resonance lines (transitions ending on the ground state). The energy lost from the plasma by radiative decay can then be predicted by summing the energy emitted in transitions from each level (omitting transitions to the ground state) and from the continuum (radiative recombination). The energy lost in the resonance line is more complicated and must be considered separately for each condition of optical thickness.

The radiated energy in a steady state plasma is provided ultimately by the electrons. This is because in the model that has been adopted the electrons produce excitation and ionization of the atoms. Hence, the radiative-energy loss rate dW_l/dt is the electron kinetic-energy loss rate. This energy must be balanced by the discharge (that is, the cathode) in order to maintain the plasma in steady state.

The radiated energy can be simply written as

$$\frac{dW_l}{dt} = - \sum_{p,q} h\nu_{pq} N(q) A(q,p) - N_e^2 \sum_{p} \int_0^\infty h\nu_p \beta(p,v) dv \ . \qquad (1)$$

The first term on the right-hand side is the line emission resulting from transitions from upper level q to lower level p at frequency ν_{pq}. The density of atoms in level q is $N(q)$, and $A(q,p)$ is the Einstein spontaneous emission rate. The second term is continuum emission by N_e electrons/cm^3 recombining with an equal density of ions. The velocity dependent recombination coefficient is $\beta(p,v)$ and ν_p is the frequency of the transitions. The frequencies are given by

$$h\nu_p = E_p = \tfrac{1}{2} mv^2$$

and

$$h\nu_{p,q} = E_p - E_q \,, \tag{2}$$

where E_p and E_q are the ionization potentials of the levels p and q. The summations are over all levels except the ground state.

The rates A and β have been discussed in previous work, and the populations $N(q)$ are given by the computer code that solves the rate equations for the atomic levels.[1,2,3] In terms of our earlier notation,

$$N(p) = R_0(p) + R_1(p)N(1) \tag{3}$$

and

$$\frac{dW_1}{dt} = - C_1 N_e^2 - C_2 N(1) \,, \tag{4}$$

where C_1 represents the contributions from the continuum and C_2 describes the energy loss resulting from excitation of the ground state $(p = 1)$.

The computer model treats 53 levels of cesium, of which the first 26 are out of equilibrium and have populations given by Eq. (3). The next 17 levels are in equilibrium and have populations given by the Saha equation. Still higher levels have negligible populations at the temperatures considered here and are neglected. In terms of these levels the coefficients C_1 and C_2 are

$$C_1 = \sum_{p=2}^{26} \left\{ \left[\sum_{q=3}^{26} (E_p - E_q) R_0(q) A(q,p) + \sum_{q=27}^{53} (E_p - E_q) N_e(q) A(q,p) \right] \frac{1}{N_e^2} + \int_0^\infty (E_p + \tfrac{1}{2} mv^2) \beta(p,v)\, dv \right\} \tag{5}$$

$$C_2 = \sum_{p=2}^{26} \sum_{q=3}^{26} (E_p - E_q) R_1(q) A(q,p) \quad . \tag{6}$$

These coefficients are dependent on the electron density and temperature. They have been calculated from solutions of the rate equations using the code prepared earlier[1,2]. Complete trapping of resonance radiation has been assumed in determining populations. The coefficients C_1 and C_2 are like the ionization rate $S(N_e,T_e)$ and the recombination rate $\alpha(N_e,T_e)$ in that they are effective rates describing the result of many transitions between levels.

In order to facilitate practical use of the results, the following empirical equations were developed for the coefficients α, S, C_1 and C_2.

$$\alpha_3 = (\alpha_o/N_e)\exp[E_a/(kT_e)^{1/2}] \qquad \text{cm}^6/\text{sec} \tag{7}$$

$$S = S_o \exp[-E_b/kT_e] \qquad \text{cm}^3/\text{sec} \tag{8}$$

$$C_1 = C_1' \exp[E_c/(kT_e)^{1/2}] \qquad \text{watt-cm}^3 \tag{9}$$

$$C_2 = C_2' \exp[-E_d/kT_e] \qquad \text{watt} \tag{10}$$

The empirical constants α_o, S_o, C_1', C_2', E_a, E_b, E_c and E_d are functions of electron density only and are tabulated in Table 1. All the temperature dependence is in the exponents. The multiplicative constants α_o/N_e, S_o, C_1' and C_2' are in the units given in Eqs. (7) - (10), while the exponential constants E_a, E_b, E_c and E_d are such that kT_e must be in eV. Linear interpolation of the values in Table 1, as a function of log N_e, will reproduce the original results to within 3% in the range $1800^oK < T_e < 3000^oK$.

It should be emphasized again that resonance radiation is not included in the emitted energy given by C_1 and C_2.

2. Energy Loss Rates in a Thermionic Converter

The energy loss rates described in the previous section have been used with the temperature and density profiles given by Reichelt[4] to deter-

TABLE I

Coefficients for use in Eqs. (7) - (10) for the calculation of effective coefficients for recombination, ionization and radiative energy loss. Complete trapping (g = 0) of resonance radiation has been assumed.

$\text{Log}_{10}(N_e, \text{cm}^{-3})$	$\alpha_o \times 10^{15}$	E_a	$S_o \times 10^5$	E_b	$C_1' \times 10^{33}$	E_c	$C_2' \times 10^{13}$	E_d
12.0	26.00	2.804	1.378	3.756	69.03	2.100	3.665	1.968
12.1	24.73	2.880	1.580	3.735	58.20	2.200	4.031	1.966
12.2	23.32	2.961	1.783	3.713	48.35	2.306	4.425	1.965
12.3	21.85	3.048	1.987	3.688	40.17	2.409	4.870	1.967
12.4	20.40	3.138	2.191	3.660	33.35	2.516	5.378	1.971
12.5	18.78	3.235	2.363	3.630	27.65	2.624	5.973	1.976
12.6	17.19	3.338	2.494	3.598	22.95	2.737	6.640	1.984
12.7	15.52	3.447	2.589	3.564	18.85	2.852	7.372	1.992
12.8	13.87	3.562	2.630	3.529	15.32	2.975	8.180	2.000
12.9	12.33	3.681	2.626	3.492	12.31	3.100	9.013	2.008
13.0	10.95	3.800	2.576	3.455	9.829	3.231	9.860	2.016
13.1	9.800	3.917	2.493	3.419	7.800	3.361	10.67	2.021
13.2	8.868	4.033	2.388	3.383	6.230	3.487	11.42	2.025
13.3	8.146	4.141	2.270	3.348	5.029	3.608	12.08	2.028
13.4	7.675	4.239	2.149	3.315	4.126	3.720	12.63	2.029
13.5	7.390	4.331	2.168	3.285	3.400	3.825	13.08	2.028
13.6	7.369	4.408	1.925	3.259	2.865	3.920	13.39	2.027
13.7	7.522	4.479	1.826	3.235	2.455	4.001	13.66	2.025
13.8	7.933	4.539	1.742	3.214	2.128	4.074	13.83	2.023
13.9	6.619	4.589	1.670	3.196	1.906	4.135	13.95	2.020
14.0	9.484	4.631	1.609	3.180	1.738	4.188	14.04	2.018
14.1	10.68	4.665	1.558	3.168	1.603	4.230	14.09	2.016
14.2	12.30	4.694	1.517	3.157	1.499	4.266	14.12	2.014
14.3	14.52	4.718	1.485	3.148	1.415	4.297	14.15	2.013
14.4	17.20	4.737	1.457	3.140	1.350	4.320	14.17	2.012
14.5	20.58	4.751	1.435	3.135	1.302	4.341	14.18	2.011
14.6	24.71	4.763	1.418	3.130	1.268	4.357	14.19	2.010
14.7	30.52	4.773	1.405	3.127	1.238	4.369	14.20	2.009
14.8	37.55	4.780	1.393	3.124	1.213	4.379	14.20	2.008
14.9	46.41	4.786	1.384	3.121	1.194	4.387	14.21	2.008
15.0	57.37	4.792	1.377	3.119	1.179	4.395	14.21	2.007

mine the actual energy lost by radiation in a typical case. The energy emitted in the resonance lines has also been included by using an approximate solution for the radiation transport equation. The lines are optically thick with considerable energy emission in the wings. The total emission has been obtained using Holstein's escape probabilities,[5] with pressure broadened line shapes in the wings.

Details of the calculation and the results have been presented at the Physical Electronics Conference, Cambridge, Massachusetts, 1967. The paper is included in the Proceedings and is reproduced as Appendix 1 of this report.

2.3 Plasma Transport Equation

The differential equations governing the transport of particles, momentum, and energy in the plasma between the electrodes of a thermionic converter have been formulated in a more complete fashion than has been done previously. Two specific advances over earlier work are the inclusion of more exact coefficients for electron transport [6] and for ion production and radiative energy loss in the plasma volume.[7]

In this section these equations are formulated and cast in a form suitable for computer integration.

The electron flux, cm^{-2}-sec^{-1}, is given by the equation[6]

$$\Gamma = - \mu_e \left[N_e E + \frac{kT_e}{e} \frac{dN_e}{dx} + \frac{N_e}{e} (\xi - 3/2)\, k \frac{dT_e}{dx} \right] \qquad (11)$$

The electron kinetic energy flux, erg-cm^{-3}-sec^{-1}, is

$$Q = \xi\, kT_e\, \Gamma - \mu_e \frac{N_e}{e} kT_e\, (\zeta - \xi^2)\, k \frac{dT_e}{dx} \qquad (12)$$

where N_e is the electron (ion) density, T_e is the electron temperature, k is Boltzmann's constant, E is the electric field, and μ_e is the electron mobility. These are standard equations, including the effect of both electron pressure and thermal diffusion.*

---

* The parameters μ_e, ξ and ζ are functions of T_e and the degree of ionization.

The equation for ion flux, cm^{-2}-sec^{-1}, corresponding to Eq. (11) is[7]

$$\Gamma_p = \mu_p \left[N_e E - \frac{kT_p}{e} \frac{dN_e}{dx} - \frac{N_e}{e} k \frac{dT_p}{dx} - K_i^T \frac{N_e}{e} k \frac{dT_p}{dx} \right] \tag{13}$$

where T_p is the ion temperature, μ_p is the ion mobility, and K_i^T is the ion thermal-diffusion constant. Since thermionic converter plasmas are characterized by relatively low degrees of ionization, the term in Ref. (8) which accounts for transfer of directed electron momentum to the ions has not been included.

In addition to Eqs. (11) - (13) continuity equations for the parameters Γ, Q and Γ_p are required. We will assume that the electron flux is constant and given by the measured current so that

$$\frac{d\Gamma}{dx} = 0 \ . \tag{14}$$

The electron kinetic-energy flux is decreased by the energy costs of ion production and radiative loss, and increased by Joule heating, expressed by

$$\frac{dQ}{dx} = - I_p \frac{d\Gamma_p}{dx} - \dot{R} - \Gamma e E \ , \tag{15}$$

where I_p is the first ionization energy of cesium and $-\dot{R}$ is the radiative energy loss. The ion production rate is

$$\frac{d\Gamma_p}{dx} = S N_e N_1 - \alpha_3 N_e^3 \tag{16}$$

where S and α_3 are the effective three-body ionization and recombination coefficients (functions of N_e and T_e), and N_1 is the density of ground-state cesium atoms.

Equations (11) - (16) are the primary equations in this formulation. If we make the assumptions that the heavy particle temperature varies linearly between the electrode temperatures, and that the ideal gas law is valid in the plasma, we can also write the equations

$$\frac{dT_p}{dx} = - (T_E - T_c)/L \tag{17}$$

and

$$N_a = \frac{P}{kT_p} - N_e \left(1 + \frac{T_e}{T_p}\right) \tag{18}$$

where T_E and T_C are the emitter and collector temperatures, respectively, P is the cesium vapor pressure, and L is the electrode spacing.

Returning to Eq. (12) the parameters μ_e, ξ and ζ are derived in Ref. (6) under the assumption that electron-electron effects are negligible. This assumption is valid for low degrees of ionization. In Ref. (6) the parameters ξ, ζ, and the effective collision frequency ν_{eff} (including both electron-atom and electron-ion effects) are presented graphically as functions of T_e and the degree of ionization N_e/N_a. The mobility μ_e is related to ν_{eff} by

$$\mu_e = \frac{e}{m\nu_{eff}} \quad , \tag{19}$$

where m is the electron mass. The graphical data of Ref. (6) have been converted to Tables 2, 3 and 4 for our use.

If we make the further assumption, based on a low degree of ionization, that the ion-ion collision frequency is much less than the ion-atom collision frequency, the ion thermal-diffusion constant[7] can be taken to be $K_i^T \simeq -0.18$. The ion mobility is related to the value at standard conditions by[9]

$$\mu_p = \mu_o \frac{N_o}{N_a}\left(\frac{T_o}{T_p}\right)^{1/2} \tag{20}$$

where $N_o = 2.69 \times 10^{19}$ atoms-cm^{-3}, $T_o = 273^oK$ and $\mu_o = 0.12$ cm^2 volt^{-1}-sec^{-1}.[8,9]

The radiative energy loss term in Eq. (15) can be written[10]

$$-\dot{R} = C_1 N_e^2 + C_2 N_1 + 5.16 \times 10^{-14}\, G\, N_1 e^{-1.432/kT_e} \tag{21}$$

where G is the geometrical factor for loss of resonance radiation. In terms of the average electrode emissivity $\bar{\epsilon}$, plasma length L, and radius R

$$G = \frac{\bar{\epsilon}}{L^{1/2}} + \frac{1}{R^{1/2}} \, . \tag{22}$$

The coefficients C_1 and C_2 are functions of N_e and T_e and are given by Eqs. (9) and (10). The coefficients S and α_3 are given by Eqs. (7) and (8).

TABLE II - ν_{eff}/N_a, (cm^3 sec^{-1})

$\log_{10} \frac{N_e}{N_a}$	T_e, °K					
	1750	2000	2250	2500	2750	3000
-3.000	4.64(-7)	4.72(-7)	4.87(-7)	5.19(-7)	5.53(-7)	5.90(-7)
-2.699	6.09(-7)	6.19(-7)	6.39(-7)	6.71(-7)	7.03(-7)	7.50(-7)
-2.301	1.000(-6)	1.016(-6)	1.049(-6)	1.083(-6)	1.118(-6)	1.173(-6)
-2.000	1.642(-6)	1.615(-6)	1.615(-6)	1.642(-6)	1.695(-6)	1.750(-6)
-1.699	2.74(-6)	2.65(-6)	2.61(-6)	2.63(-6)	2.66(-6)	2.70(-6)
-1.301	5.62(-6)	5.27(-6)	5.03(-6)	4.87(-6)	4.72(-6)	4.64(-6)
-1.000	1.033(-5)	9.08(-6)	8.39(-6)	7.87(-6)	7.38(-6)	7.03(-6)

TABLE III - ζ, Dimensionless

$\log_{10} \frac{N_e}{N_a}$	T_e, °K					
	1750	2000	2250	2500	2750	3000
-3.000	6.71	5.48	4.71	4.20	3.85	3.73
-2.699	7.01	5.82	5.01	4.58	4.24	4.11
-2.301	7.57	6.46	5.73	5.30	5.09	5.13
-2.000	8.29	2.27	6.63	6.33	6.20	6.37
-1.699	9.32	8.42	7.91	7.74	7.78	8.08
-1.301	11.24	10.55	10.26	10.34	10.60	11.07
-1.000	13.03	12.56	12.43	12.65	12.99	13.50

TABLE IV - ξ, Dimensionless

$\log_{10} \frac{N_e}{N_a}$	T_e, °K					
	1750	2000	2250	2500	2750	3000
-3.000	2.46	2.23	2.04	1.89	1.78	1.70
-2.699	2.50	2.27	2.09	1.94	1.84	1.77
-2.301	2.58	2.36	2.19	2.07	1.98	1.93
-2.000	2.68	2.48	2.32	2.22	2.15	2.12
-1.699	2.81	2.64	2.51	2.43	2.39	2.38
-1.301	3.05	2.91	2.82	2.78	2.77	2.80
-1.000	3.25	3.16	3.09	3.08	3.09	3.13

The pressure P, dyne-cm^2, in Eq. (18) is related to the cesium reservoir temperature, T_{Cs}, by the Langmuir equation

$$P = 1.332 \times 10^3 \, T_{Cs}^{-1.35} \, 10^{11.0531 - 4041.0/T_{Cs}} \quad . \tag{23}$$

The ground state density and total atom density are related by $N_1 = \Pi N_a$, where Π is the partition function for cesium

$$\Pi = 2 \, e^{I_p/kT_e} / \sum_{i=1}^{\infty} g_i \, e^{I_i/kT_e} \quad . \tag{24}$$

The statistical weights and ionization energies of the bound levels of cesium are g_i and I_i, respectively.

It is more convenient to use the Einstein relation

$$\mu = \frac{eD}{kT} \tag{25}$$

in rewriting Eqs. (11)-(13). After some algebra, the transport equations can be transformed to the form

$$\frac{dT_e}{dx} = \frac{\xi k T_e \Gamma - Q}{(\zeta - \xi^2) k N_e D_e} \tag{26}$$

$$\frac{dN_e}{dx} = - \frac{T_e}{T_e + T_p} \left\{ \frac{\Gamma}{D_e} + \frac{T_p}{T_e} \frac{\Gamma_p}{D_p} + \frac{N_e}{T_e} \left[\left(1 + K_i^T \right) \frac{dT_p}{dx} + (\xi - 3/2) \frac{dT_e}{dx} \right] \right\} \tag{27}$$

$$\frac{d\Gamma_p}{dx} = S N_e N_1 - \alpha_3 N_e^3 \tag{28}$$

$$\frac{dV}{dx} = - E = - \frac{kT_p}{eN_e D_p} \left[\Gamma_p + D_p \frac{dN_e}{dx} + \frac{D_p}{T_p} N_e \frac{dT_p}{dx} \right] \tag{29}$$

$$\frac{dQ}{dx} = - I_p \frac{d\Gamma_p}{dx} - R - \Gamma E e \tag{30}$$

$$\frac{dT_p}{dx} = - (T_E - T_C)/L \tag{31}$$

3.0 DIODE EXPERIMENTS

3.1 Objectives

The objectives of the spectroscopic work are to provide further data on the spatial variation of electron temperature and density across the interelectrode gap of a converter for experimental verification of the non-equilibrium calculations and to explore features of the spectrum that may be used for refined diagnostic measurements. In addition, ionization cross sections have been measured, with particular emphasis on the threshold behavior.

3.2 Principles of Spectroscopic Measurements

3.2.1 Recombination Intensities. Electron temperatures have been determined from measurement of the continuum emitted by radiative recombination to the 6P states of cesium. The reaction is

$$Cs^+ + e \rightarrow Cs(6P) + h\nu \qquad (32)$$

The 6P is commonly used because it is usually the strongest continuum and it is in a region of the spectrum that is relatively free from lines. The intensity distribution of the continuum enables the determination of the electron temperature using only relative intensity measurements.[11]

The intensity distribution has its threshold at about 5080 $\mathring{A}$ and is given by

$$I(\lambda)d\lambda = h\nu N_e N_i v\, \sigma(v) f(v) dv \qquad (33)$$

where $I(\lambda)d\lambda$ is the emission rate (erg/cm^3-sec) in the wavelength interval $d\lambda$ about λ, corresponding to electrons in the velocity interval dv about v, σ is the velocity-dependent cross section for recombination to the 6P level and $f(v)dv$ is the fraction of electrons in dv about v. The most recent values for the cross section are due to Agnew and Summers[12]

$$\sigma_{A+S}(v) = \frac{3.74 \times 10^{-6}}{v^2} \text{ cm}^2 . \qquad (34)$$

These compare with earlier measurements by Mohler[13] of

$$\sigma_M(v) = \frac{2.26 \times 10^{-6}}{v^2}\left(\frac{\lambda}{5080}\right)^2 \quad cm^2 \tag{35}$$

where λ is the wavelength in Angstroms. The electron velocity v is in cm/sec in both equations.

The Agnew and Summers cross section is more correct, since it was obtained from measurements of an equilibrium system (isothermal). Their cross section and a Maxwell distribution of velocities in Eq. (33) gives

$$I(\lambda) = 3.74 \times 10^{-6}\, N_e N_i \left(\frac{2m}{\pi}\right)^{1/2} \frac{(hc)^2}{(kT)^{3/2}} \frac{1}{\lambda^3} e^{-E/kT} \tag{36}$$

or

$$\ell n[\lambda^3 I(\lambda)] = K - 3/2\ \ell nT - E/kT\ ,$$

where K is a constant and E is the energy above the series limit. Since the temperature is constant during recording of the spectrum, a plot of $\ell n[\lambda^3 I(\lambda)]$ vs E gives a straight line with a slope of $-1/kT$. If the Mohler cross section is used, the logarithmic equation is

$$\ell n[\lambda I(\lambda)] = M - 3/2\ \ell nT - E/kT\ , \tag{37}$$

where M is a different constant. The only important change here is the power of λ multiplying $I(\lambda)$ on the left side. Over the small wavelength range observed in typical experiments (4000 - 5000 Å) the Mohler cross section gives temperatures greater by about 15%. Equation (36) is preferred.

The recombination continuum can also be used to determine electron density. In this case absolute measurement of the intensity $I(\lambda)$ must be made. Equation (33) is then solved for $N_e N_i$ using the temperature from the relative shape of the continuum to obtain $F(v)$. The ion and electron density can be assumed equal in most converters, so N_e is determined. Mohler's cross section in this case gives densities about 35% higher than those obtained from Agnew and Sommer's cross section. The absolute measurement is rather difficult to perform and is subject to absorption errors. As a result, the more easily performed and less sensitive line shape measurement is considered more reliable.

3.2.2 Line Shapes. Line shapes give densities when the lines are predominantly Stark broadened as opposed to other broadening mechanisms. In such a case the width is nearly directly proportional to the electron density. The widths have been worked out in detail[14,15] and verified experimentally.[13] The basic mechanism that results in broadening is the shift of the levels of the radiating atom due to the electric field (Stark effect) of the electrons and ions of the plasma. The shift is averaged over the distribution of electron and ions around the radiating atom and results in a broadened (and shifted) line. The theory has been developed for isolated lines so that the broadening must not be so large that lines overlap.

In practice the fundamental series lines are most suitable for Stark broadening measurements. Over a density range from 10^{13} - 10^{15} electrons/cm^3 the lines are isolated and sufficiently wide that their shape can be determined with low resolution spectrometers. The shapes are only slightly temperature dependent (a few percent for cesium over temperatures from 2000^{0}K to 5000^{0}K) and so the temperatures need not be known to determine electron density. The density is determined in practice by measuring the widths of several fundamental series lines at half maximum intensity and comparing with calculated values.

3.3 Experimental Procedure

The diode was run at a constant body and emitter temperature and with constant gas flow to the collector seal. The cesium density was adjusted by varying the reservoir temperature. This was done from low to high, always keeping it enough lower than all other sections so that it was the controlling element. A factor of two increase in pressure, which required a rise of about 25^{0}C, would stabilize in 15 minutes. The temperature was controlled by varying the current through the diode. In this case stabilization was almost instant and a run could be repeated after five minutes. The diode current control circuit is shown in Fig. 1.

Stability was verified by peaking the monochrometer manually on any of the lines of interest and running for five minutes with zero drift. Emitter temperature was monitored continuously with a two color optical pyrometer. This device takes the ratio of the color temperature at two different bands of wavelengths in the visual spectrum. This helps to correct for variations in emissivity of the emitter. The area of the emitter viewed was

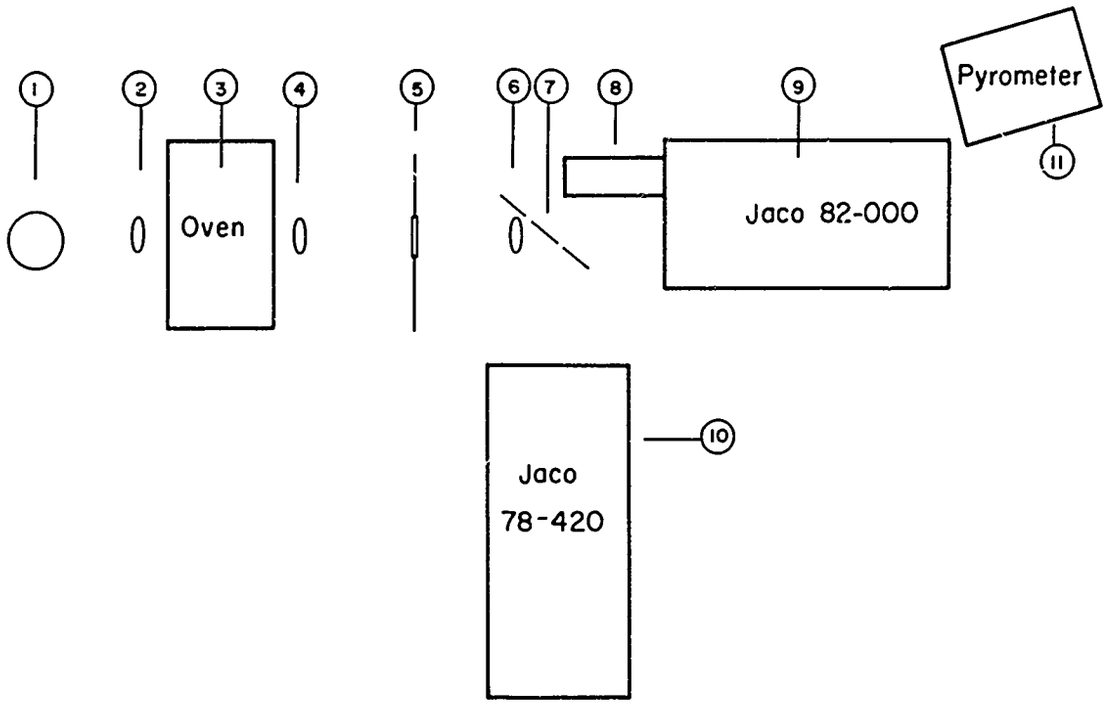

1. STANDARD LAMP
2. 15 mm LENS
3. DIODE OVEN
4. 15 mm LENS
5. MICROMETER WINDOW
6. 15 mm LENS
7. FRONT SILVERED MIRROR MOVEABLE
8. EMI 9558A P.M. WITH MAGNETIC LENS
9. JACO 82-000 1/2m MONOCHROMETER
10. JACO 78-420 1m MONOCHROMETER
11. PYROMETER

FIG. 1 Optical bench layout.

a spot 0.1" in diameter on the center line of the sleeve immediately behind the emitter button. The weld line where the button was attached to the sleeve was used as the reference for one edge of the area viewed. This gave continuous monitoring without any influence from the plasma except at the lowest densities at which measurements could be made.

Calibration for the measurement of relative and absolute line intensities was made by replacing the diode with a tungsten strip lamp calibrated as a standard of spectral radiance by NBS (Fig. 2). This substitution procedure obviated the need for corrections due to reflection losses, variation in solid angles, etc. All line intensity measurements and the majority of the line broadening measurements were made using a 0.5 meter scanning monochrometer (Jarrell-Ash Model 82-000) equipped with a 15,000 lpi grating. For the measurements of forbidden line intensities and shapes and resonance line shapes a 1.0 meter scanning monochromator (Jarrell-Ash Model 178-420) was employed. This instrument was equipped with a 30,000 lpi grating blazed at 1 μ . A bandpass of better than 0.03 $\mathring{A}$ (3rd order) was demonstrated with this instrument. This monochromator was also used to check the line shapes measured with the lower resolution spectrometer. Little or no correction for instrument width was required.

Since one of the objectives of this study was to measure recombination temperatures at low electron densities ($< 10^{13}/cm^{-3}$), considerable effort was expended to maximize the signal-to-noise ratio of the system. Phase sensitive detection was tried but the high time constants which are required in this technique made it unsuitable for our purposes. The most successful technique was the use of a magnetic lens (Fig. 3). This consists simply of a 200 ampere-turn coil coaxial with the photocathode of the EMI 9558 A photomultiplier tube. This had the effect of reducing the system noise by a factor of 100 while increasing the signal about 15%. This arrangement provided the requisite sensitivity for the measurement of the low light levels encountered.

3.4 Temperature and Density Spatial Distributions

The external optical system allowed the interelectrode plasma to be focused on the entrance slit of the monochromator with a magnification

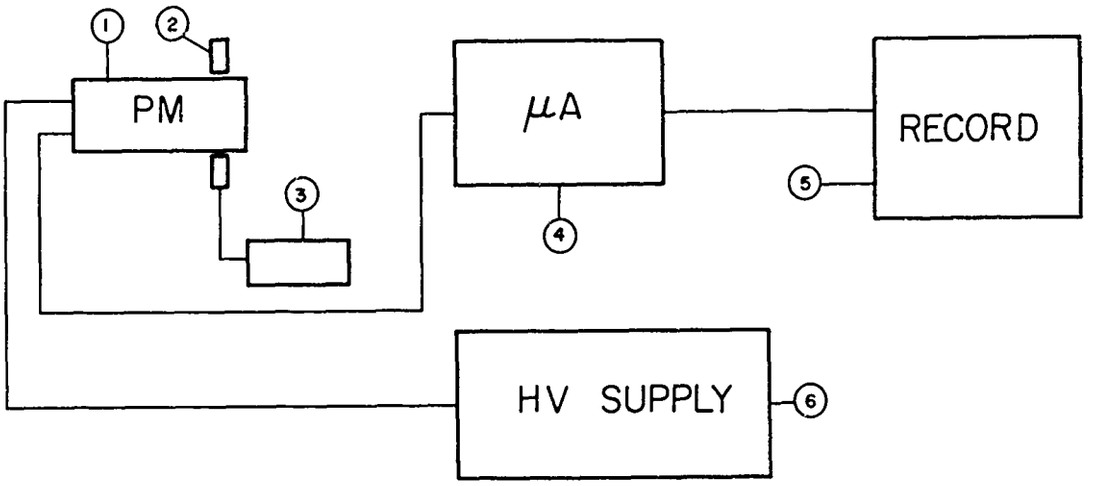

1. EMI 9558A
2. MAGNETIC LENS
3. LENS SUPPLY
4. KIETHLY MOD 410 MICRO MICROAMMETER
5. L & N SPEEDOMAX G. RECORDER
6. KIETHLY MOD. 242 REGULATED HIGH VOLTAGE SUPPLY

FIG. 2 Photomultiplier detection system.

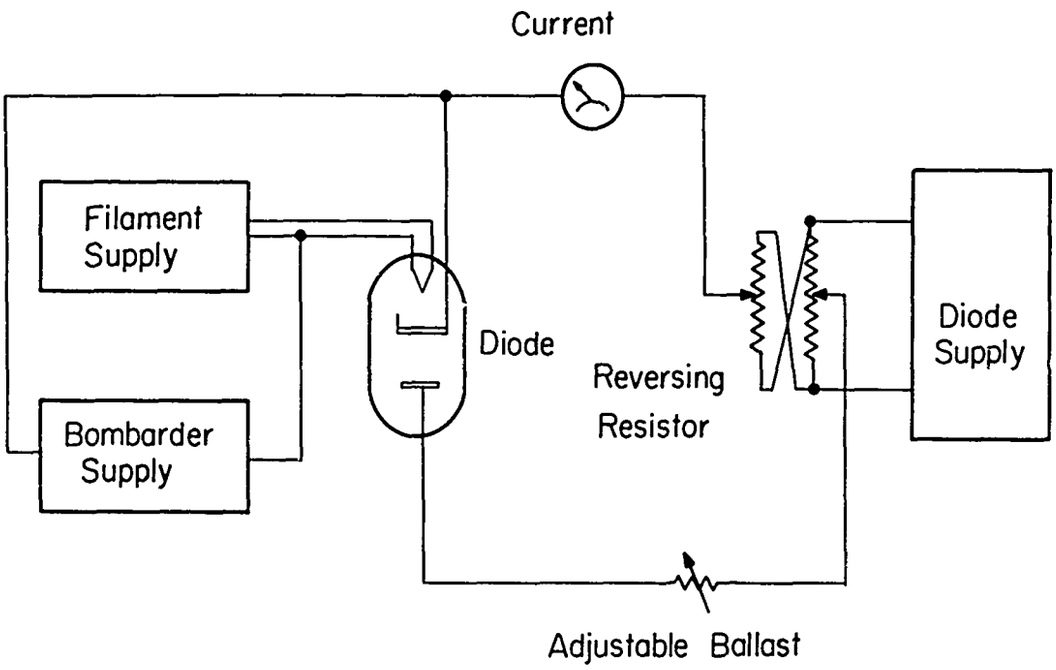

FIG. 3 Diode current control.

of 5.5X. The monochromator itself was mounted on tracks which allowed it to be moved transverse to the optical axis with a precision of 0.1 mm. This allowed spatially resolved spectral measurements to be made. In this manner the temperature and electron density profiles shown in Figs. 4 and 5 were obtained. As in all of this work, the densities were measured by observing the half width of the 8F - 5D transition at 6628 Å. This half width was related to the density in the manner described above. Temperatures were measured by measuring the intensity variation of the recombination continuum as described above. Four points at 100 Å intervals from 5000 Å to 4700 Å were measured for the data reported here. Later measurements increased the lower wavelength range to 4300 Å but did not alter the conclusion significantly. (These data are too incomplete for inclusion here.) The recombination data was reduced by computer. At the same time the temperatures were obtained, density data were also generated because an absolute calibration of the optical system was available. These density measurements were not in satisfactory agreement with the densities measured using line width. The latter densities are considered more accurate, since less precise measurements are required in obtaining them and the line broadening technique is well established. The difference appears to be due to extraneous radiation in the gap, but time did not permit a definitive study of this problem.

3.5 Resonance Line Shapes

Resonance lines have been observed in emission under a variety of plasma conditions. They are self-absorbed because of the cold gas outside the plasma region. However, they have a characteristic asymmetry, as shown in Fig. 6. There appears to be a shift of the emission line relative to the absorption line of the cold gas and also an asymmetry of either the absorption or emission line, or both.

The resonance absorption lines have also been measured by shining a standard lamp through the cold cesium gas with the diode turned off. Figures 7 and 8 show the shapes of the 6S - 7P doublet lines as pressure is varied. The lines have very surprising asymmetry. The cause is not clear, but is probably due to small collisional broadening of the line. The effect is magnified in an optically thick gas as the two wings of a line have different absorption and saturate at different optical thicknesses.

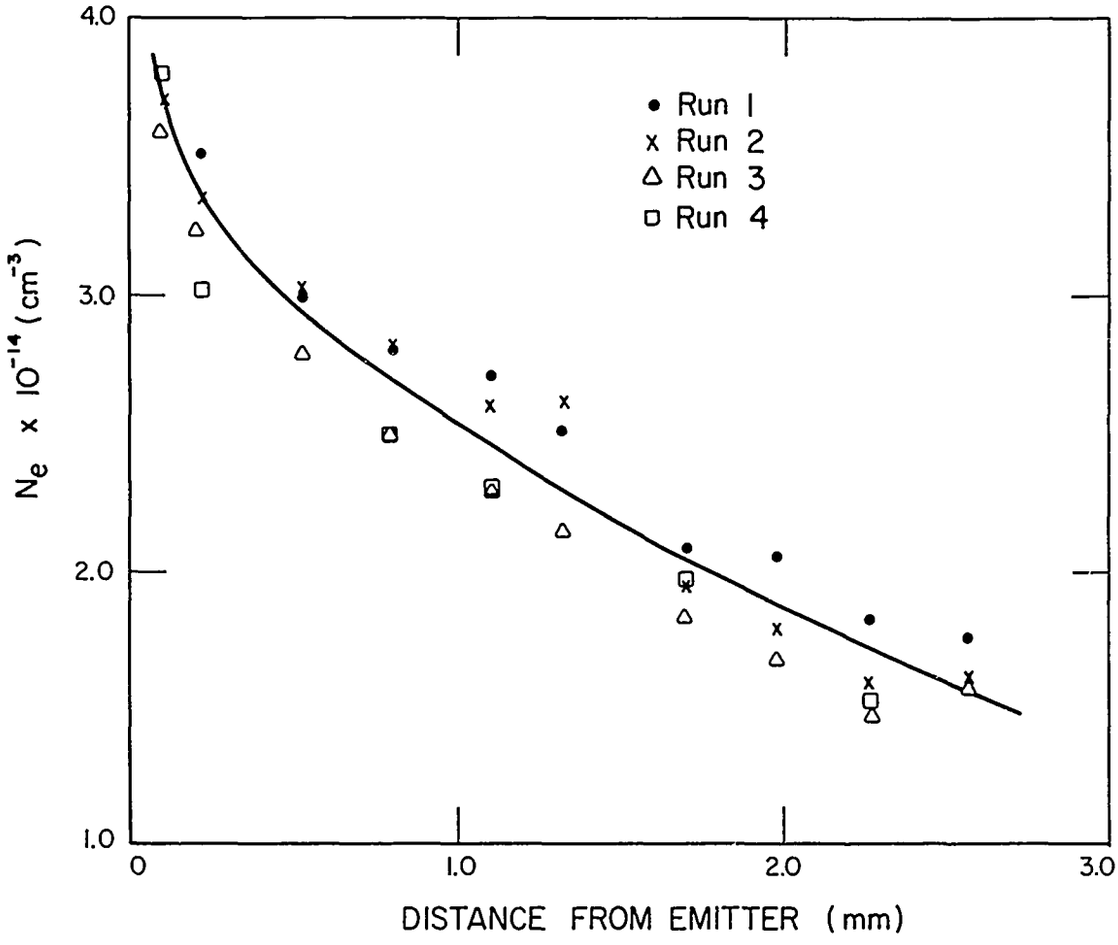

FIG. 4 Measured electron density distribution across the interelectrode gap. The density is determined from the Stark broadening of the 6628 Å (8F - 5D) line. The corresponding electron temperature is shown in Fig. 5.

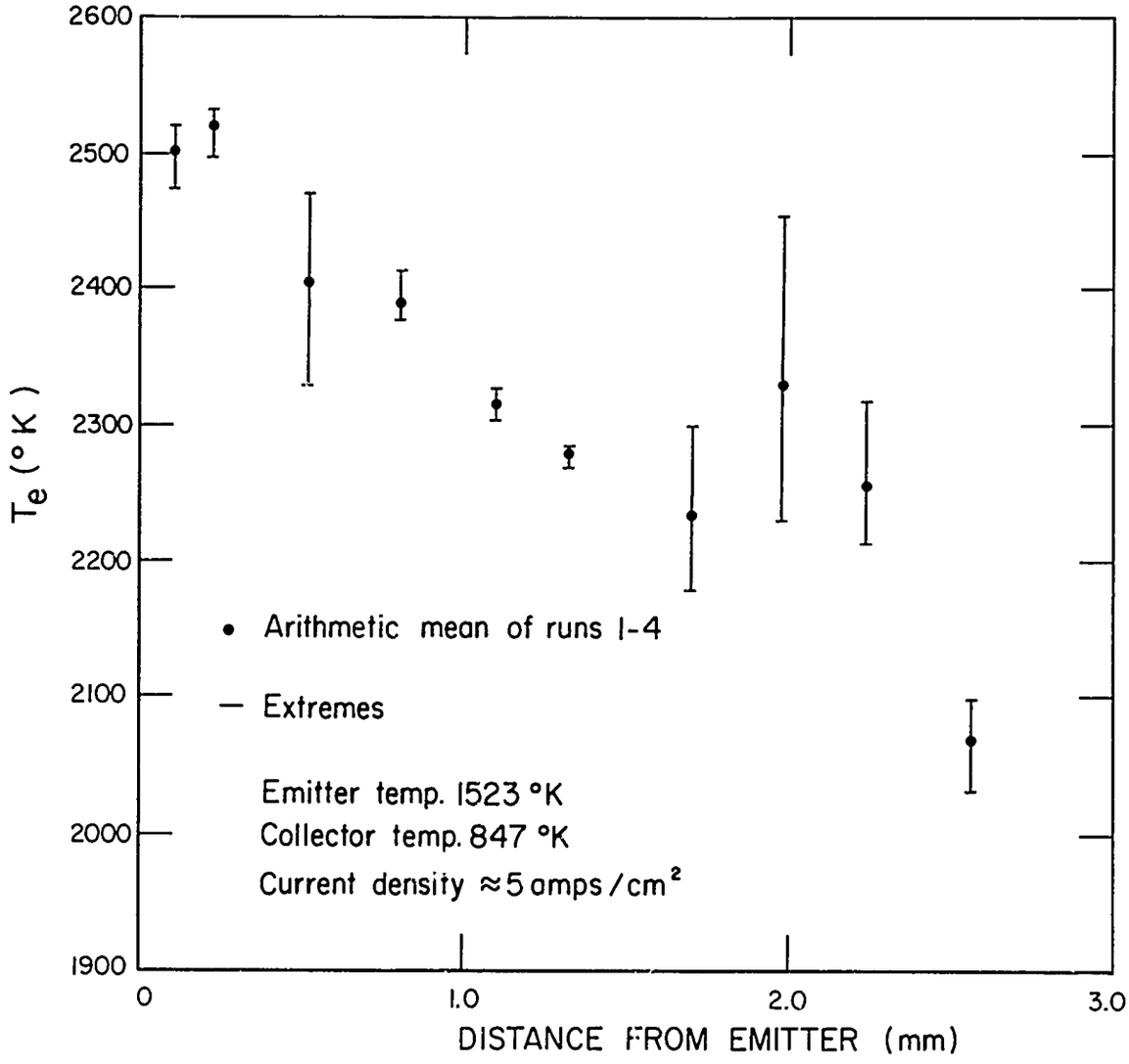

FIG. 5 Measured electron temperature distribution across the interelectrode gap. The temperature is determined from the recombination spectrum using the cross section of Agnew and Sommers (see text). The arithmetic mean of four runs is plotted. The corresponding electron densities are shown in Fig. 4.

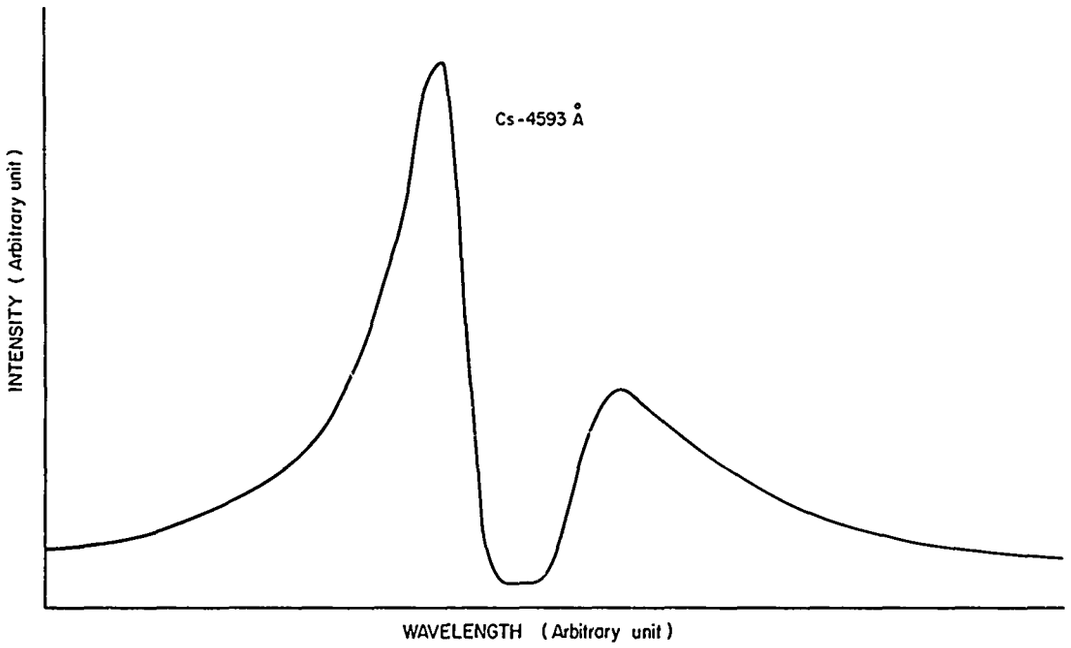

FIG. 6 Shape of the Cs-4593 Å line in emission.

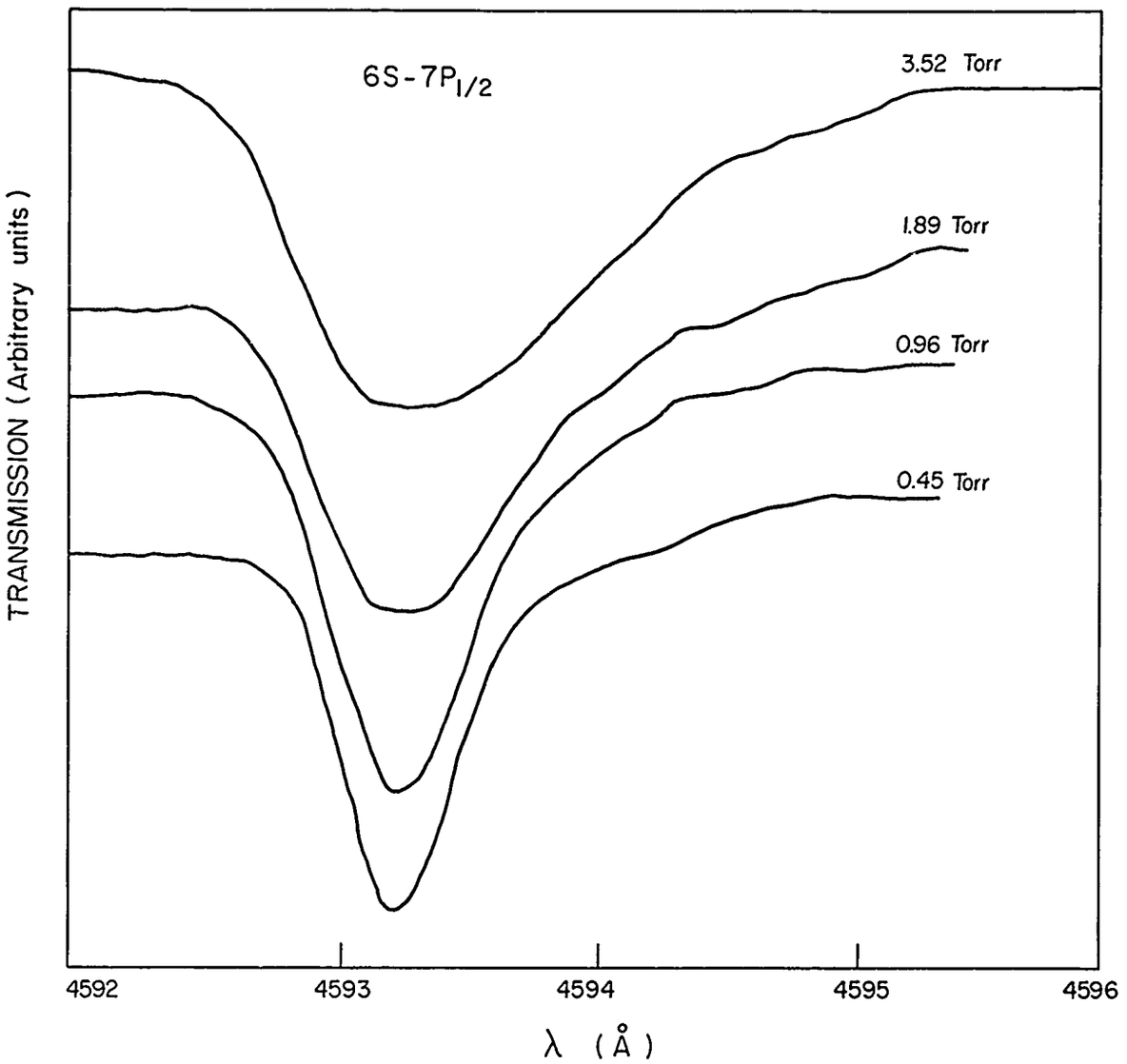

FIG. 7 The 4593 Å resonance absorption line at different pressures.

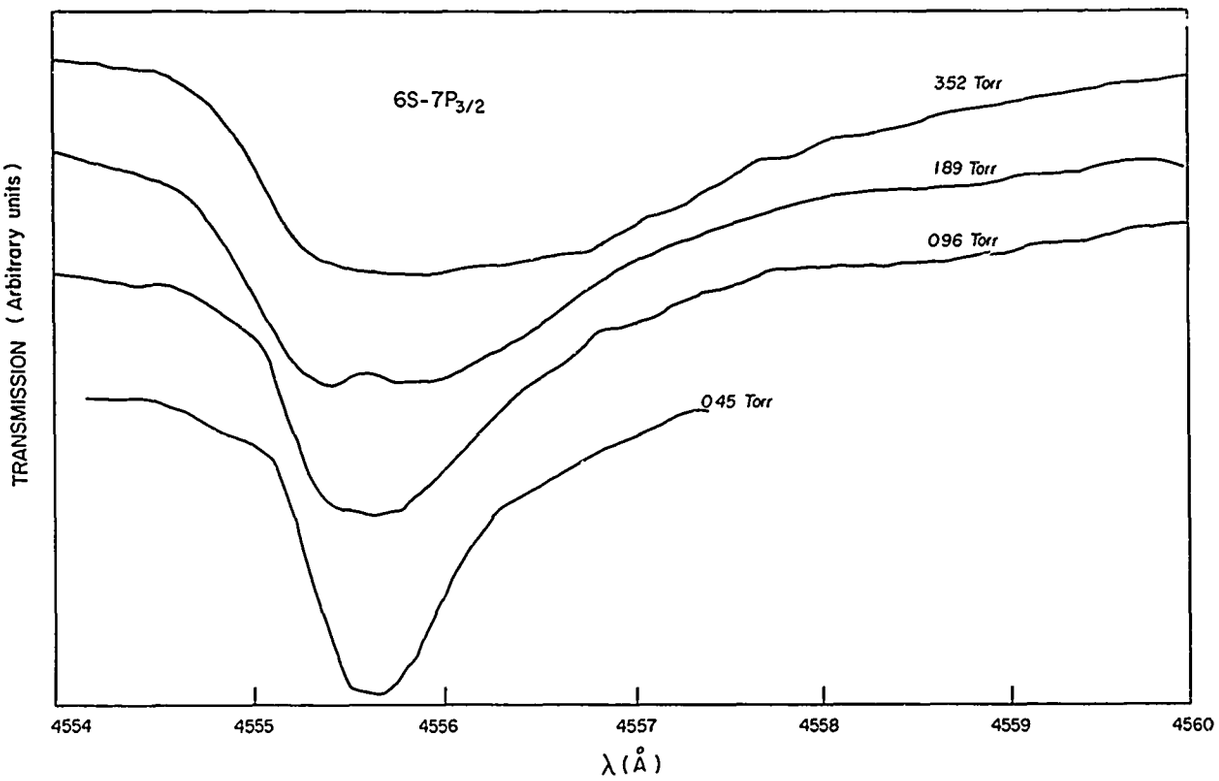

FIG. 8 The 4556 Å resonance absorption line at different pressures.

3.6 Forbidden Line Intensities

On the low wavelength side of the Stark broadened fundamental series lines (5D - nF), relatively weak "forbidden" lines of the 6F - 5D series are observed. The forbidden and allowed lines are well separated for transitions to the lower F levels and become stronger and closer together for transitions to higher F levels. The 6G - $5D_{5/2}$ transition (7269 Å) at an electron density of $1.5 \times 10^{14} cm^{-3}$ is shown in Fig. 9. The allowed 6F - $5D_{5/2}$ line at 7279 Å has a peak intensity well above the top of the paper. The same line at two higher electron densities is shown in Fig. 10. The electron densities have been determined from Stark broadening measurements of the 6628 Å (8F - $5D_{5/2}$) line.

The forbidden line has definite structure in the center and very sharp fall-off in the wings. The center appears to be made up of two lines slightly displaced, giving a double peak. As the density is increased, the line becomes broader, the total intensity increases, and the double-peak structure is lost.

Considerable data were taken of the total intensity of the forbidden line as the density was varied. These results for the 7270 Å (6G - $5D_{5/2}$) lines are shown in Fig. 11. The intensity of this line divided by the intensity of the allowed 6034.09 Å ($10S_{1/2}$ - $6P_{3/2}$) line is plotted against electron density. Division by the intensity of the 6034.09 Å line has been done to eliminate temperature effects that change intensities as density is varied. The upper state of the 6034.09 Å line ($10S_{1/2}$) lies very near the upper state of the forbidden line (6G). Therefore, population changes as the temperature is varied are the same for both lines and the ratio should be independent of temperature.

Figure 11 shows a linear increase of total intensity with density until about 4.2×10^{14} cm^{-3}. Thereafter, the intensity continues to increase linearly but at a lower rate. The density at this rather abrupt change in slope is approximately where the double-peak nature of the forbidden line disappears.

The forbidden lines are present because of the electric field (Stark effect) of the ions and electrons in the plasma. These fields destroy atomic degeneracy of levels and shift the energies of the levels. The theory

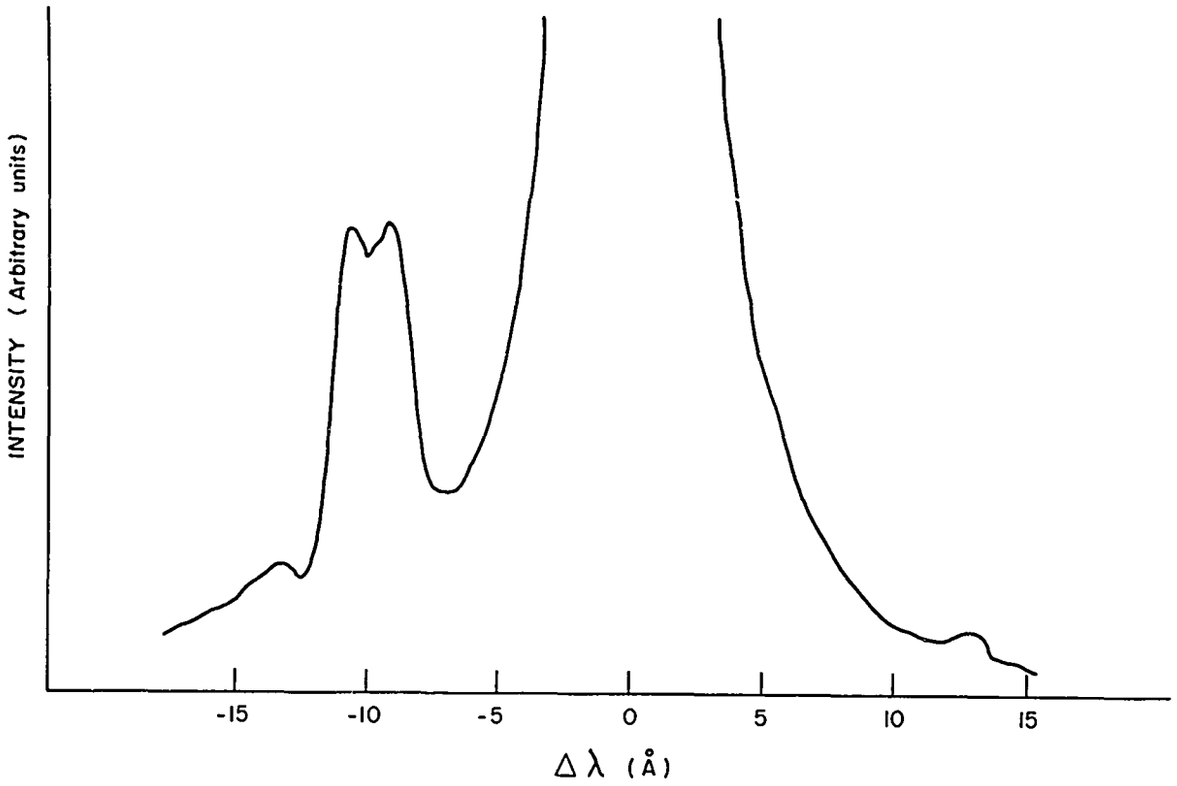

FIG. 9 Forbidden line profile of 7269 Å ($6G - 5D_{5/2}$) on wing of the allowed 7279 Å ($6F - 5D_{5/2}$) as measured with the high resolution instrument. $N_e = 1.5 \times 10^{14}$ cm^{-3}; $T_e \approx 2000^{\circ}$K.

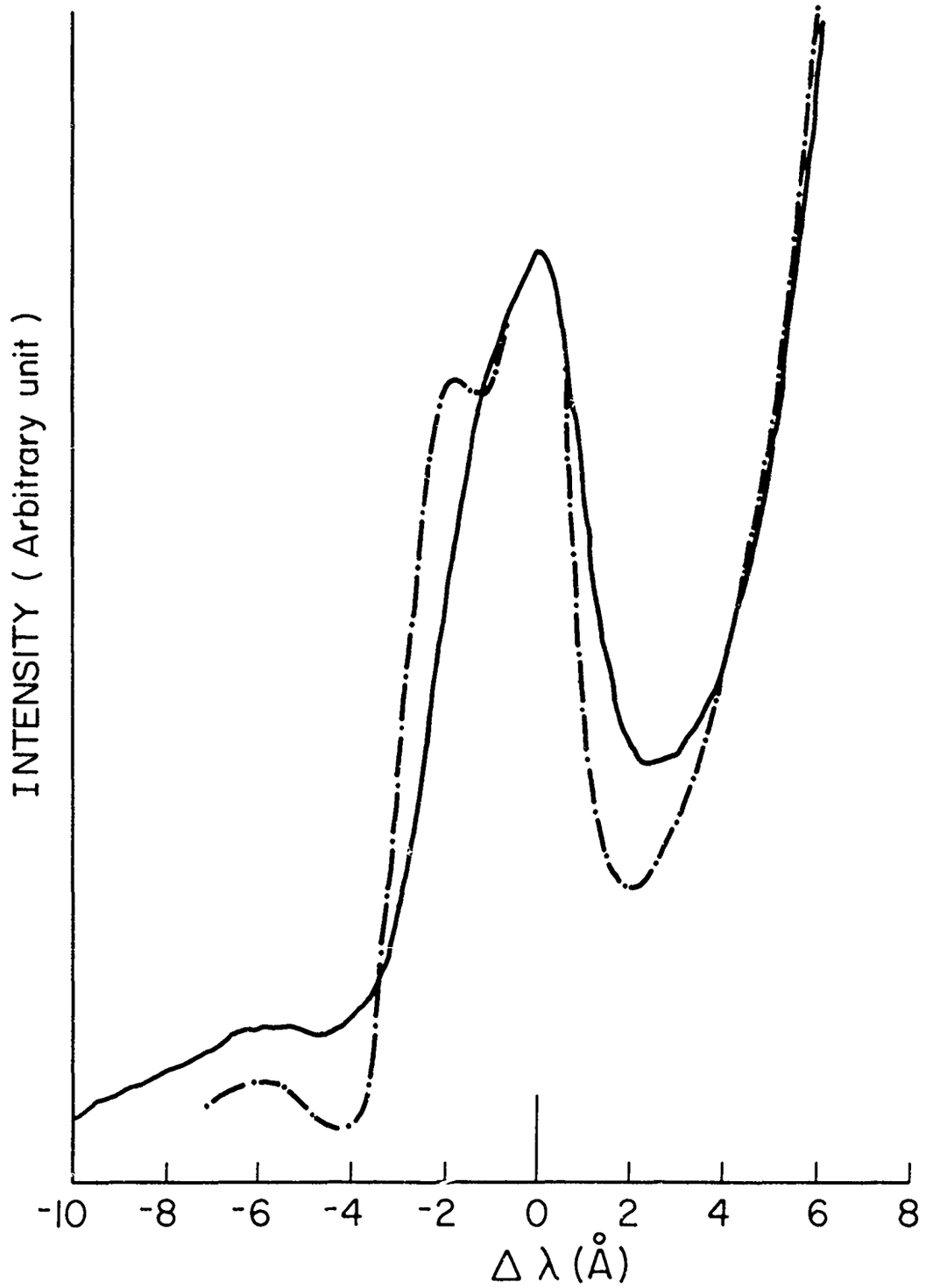

FIG. 10 The 7269 Å forbidden profile showing the effect of electron density. $N_e = 4.85 \times 10^{14}$ for solid line and 2.20×10^{14} cm^{-3} for broken line. $T_e \approx 2000^{o}K$.

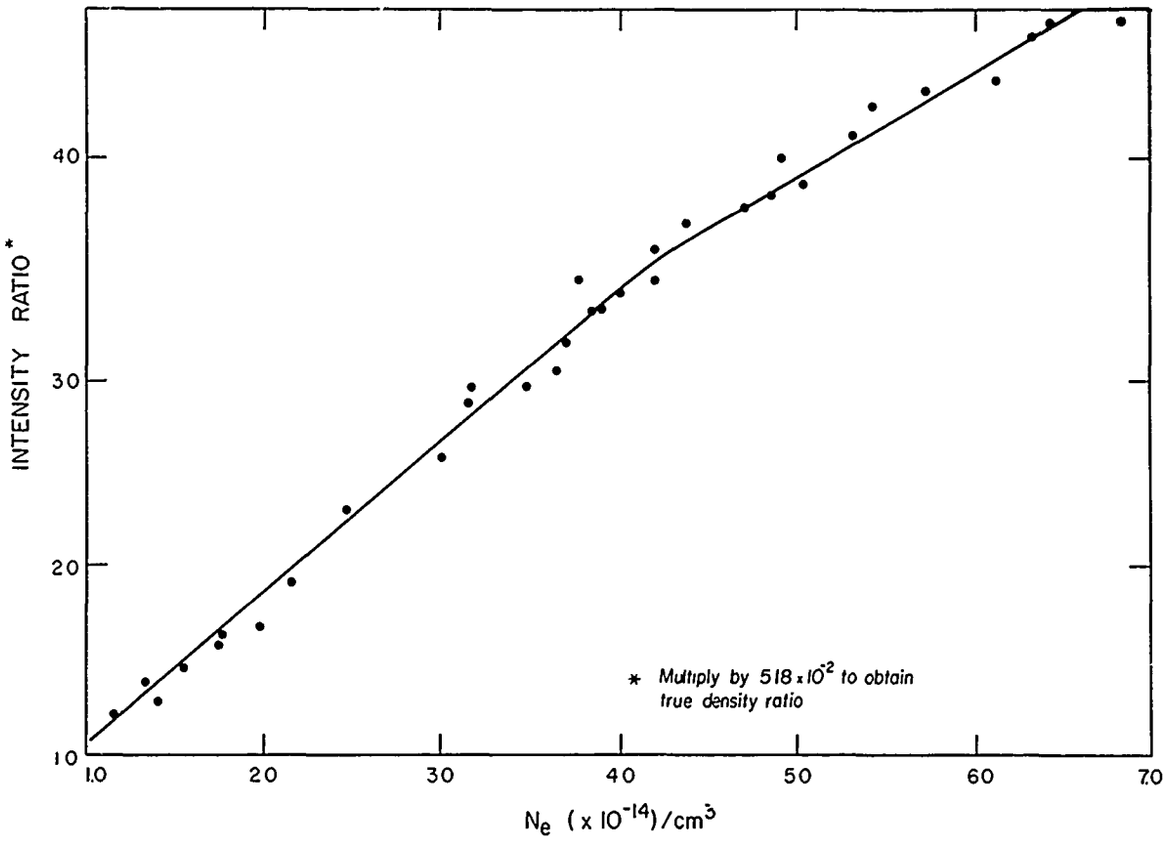

FIG. 11 Intensity ratio of Cs 7269 Å ($6G - 5D_{5/2}$)/Cs 6034 Å ($10S_{1/2} - 6P_{3/2}$) vs N_e measured by broadening of Cs 6628 Å ($8F - 5D_{5/2}$).

is quite analogous to the Stark broadening theory of lines, and the forbidden lines are a second manifestation of the plasma forces.

Some theoretical work has been done on forbidden line intensities in plasmas,[16] but only for isolated lines. Isolated lines do not overlap other lines; in an element like cesium this means that the upper level of the line is not degenerate with any other level. Unfortunately, the transitions discussed here are not isolated because the upper level, 6G, is degenerate with 6H and 6I. Therefore, hydrogenic theory (levels degenerate in ℓ) must be used rather than isolated line theory. This has not yet been worked out.

The double peaks of the 5D - 6G lines are probably a result of the degeneracy of the 6G and 6H levels. Splitting into double peaks is characteristic of Stark broadening of degenerate levels and is very pronounced in hydrogen. The disappearance of the double peaks as density is increased is quite likely a result of the broadening of each of the two lines result in the observation of one peak.

The data of Figs. 9 - 11 is the first quantitative data of forbidden non-isolated line intensities induced by plasma effects. Theoretical explanation of the intensities and shapes will be a critical and needed test of Stark broadening theory. Moreover, the mere presence of forbidden lines is a rough indication of density, and their observation can serve as a quick diagnostic measurement. Quantitative density determinations can be obtained from curves such as Fig. 11, and such measurements serve as an alternative to Stark broadening measurements.

4.0 ELECTRON IMPACT IONIZATION CROSS SECTION IN CESIUM

4.1 Present Status

The interpretation of many plasma experiments using cesium (for instance thermionic energy converters, ion propulsion devices, and vapor release in the atmosphere), rests upon a full understanding of the various mechanisms of ionization. The objective of our work has been to determine the cross section for ionization of cesium atoms by electrons. Optical absorption measurements by Kratz[17] have given the series limit in cesium at 3.8926 eV. Electron beam measurements agree with this value, but are, of course, not as accurate. The efficiency of ionization (in arbitrary units) of the cesium atom by electron bombardment was first measured by Tate and Smith[18] with energies ranging from threshold to 700 eV. They discriminated between singly- and multiply-charged ions with a mass spectrometer. The absolute magnitude of the cross section was first determined in the crossed-beam experiment of Brink,[19] followed by more measurements in another apparatus of the same type by McFarland and Kinney.[20] In the crossed-beam experiments the data were obtained for energies between 30 and 500 eV in steps of 100 eV above 100 eV. These high-energy results were later supplemented by the threshold and low-energy measurements of Heil and Scott[21] (up to 50 eV) and Korchevoi and Przonski[22] (up to 25 eV), who all used systems in which cesium vapor was in thermodynamic equilibrium with a liquid-phase reservoir.

The ratio between the highest[19,20,22] and lowest[21] maximum cross-section values reported is about a factor of two. The reasons for this discrepancy are not completely understood. On this basis, we found it desirable to make a new determination of the ionization cross section from threshold to 100 eV in order to get an overlap between the low- and high-energy measurements discussed above.

We used a Tate and Smith[18]-type apparatus modified to include the feature of retarding potential difference[23] (RPD) in the electron gun. It is crucial that the number density of cesium atoms in the collision region be accurately known. Measurements with a surface ionization detector[24] yielded density values that agreed with those calculated from the formulas of Taylor and Langmuir[25] within $\pm$ 3%.

4.2 Experimental

4.2.1 General - The major components of the experiment are shown in Fig. 12. The electron gun and ionization region (to be described later) are located in the middle of a vertically hanging tube with a pool of cesium at the bottom. The cross in the wide pump-out tube contains an ionization gauge for measuring background pressure during baking and pumping and a surface ionization detector for determination of cesium density. The vacuum parts are all made from stainless steel and copper. During bake-out, the vertical tube, valves V_1 and V_2, and the VacIon pump to the left are all heated to 300^0 - 400^0C while pumping is done with the other VacIon pump. Cesium[26] is then evaporated into the pool through a small side-arm (not shown in the illustration). Under normal operation the high-vacuum valves are closed, and the "clean" VacIon pump to the left in Fig. 12 acts on the experimental volume through a small-diameter copper tubing from the cesium pool. Part of this tube is water-cooled to about 35^0C in order to prevent cesium from entering the pump. An end vacuum of 10^{-9} torr is easily obtained after the bake-out procedure. The apparatus shown in Fig. 12 can be moved up and down as one unit, which facilitates the lowering of the tube into a solenoid. Circulating hot air keeps the temperature of the tube and the valve V_1 at about 120^0C, thereby avoiding undesirable cold spots where the cesium could condense. The temperature of the Cs pool is kept constant to within $\pm$ 0.05^0C by means of a thermostatically controled closed loop of oil. Notice that Cs atoms effuse out of the lower orifice of the small-diameter pumping tube with the temperature T_{Cs}, since this part of the tube is immersed in the oil bath. The length immersed was actually helix-shaped, thereby making the constant-temperature region much longer than indicated in Fig. 12. It is also important that the diameter of the pump-out tube be much smaller than the diameter of the cesium pool.

4.2.2 Cross Section Apparatus - The electron gun in Fig. 13 was constructed according to the RPD principle of Fox et al.[23] All electrodes were made from copper. Electrons were emitted from an indirectly heated Philips cathode of type A. The emission current from this cathode in the presence of cesium was found to be very stable, so that stabilization of the current by electronic means was unnecessary.

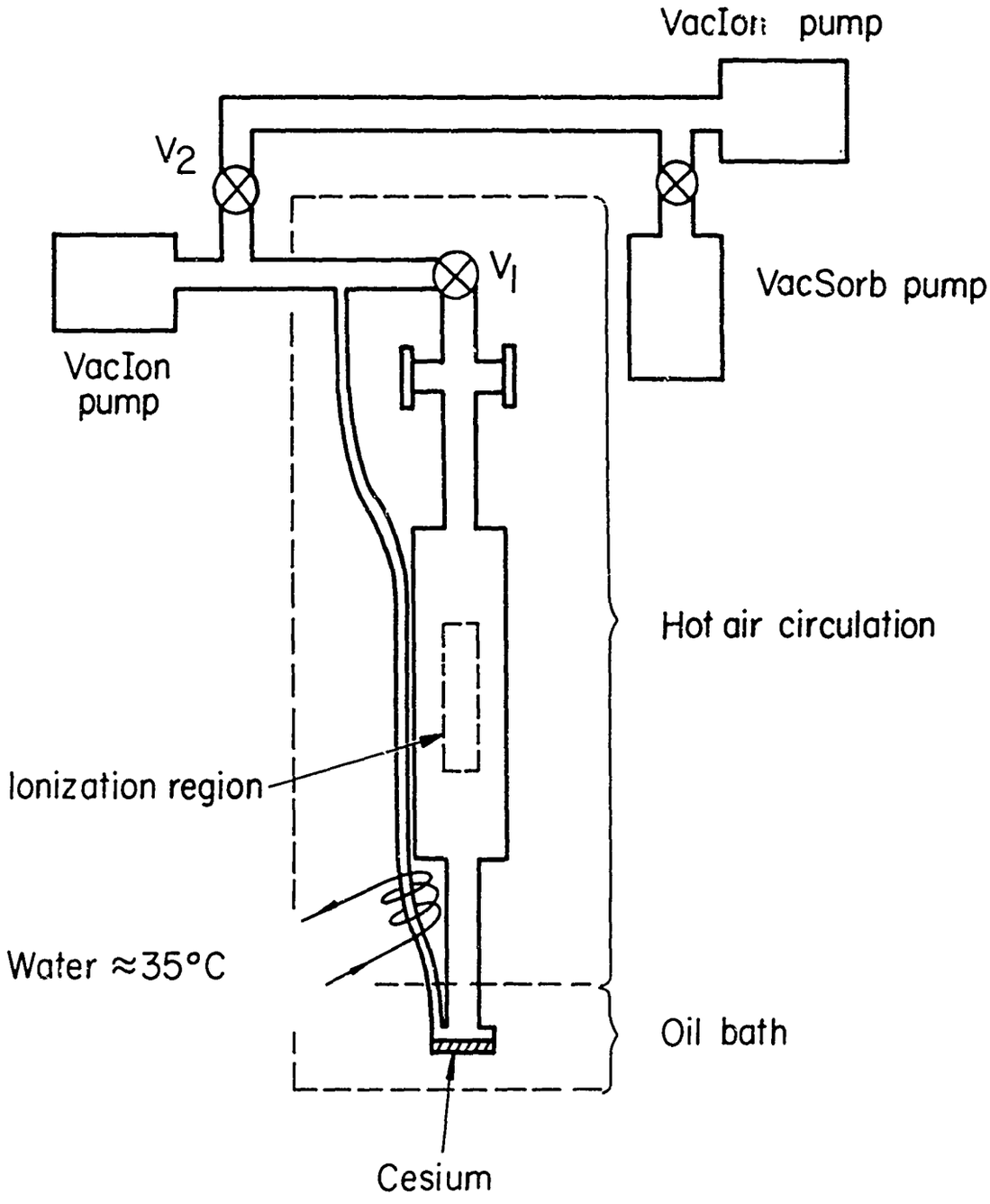

FIG. 12 Schematic diagram of vacuum system and cesium reservoir. Surface ionization detector and ionization gauge are mounted on the two flanges above the ionization region.

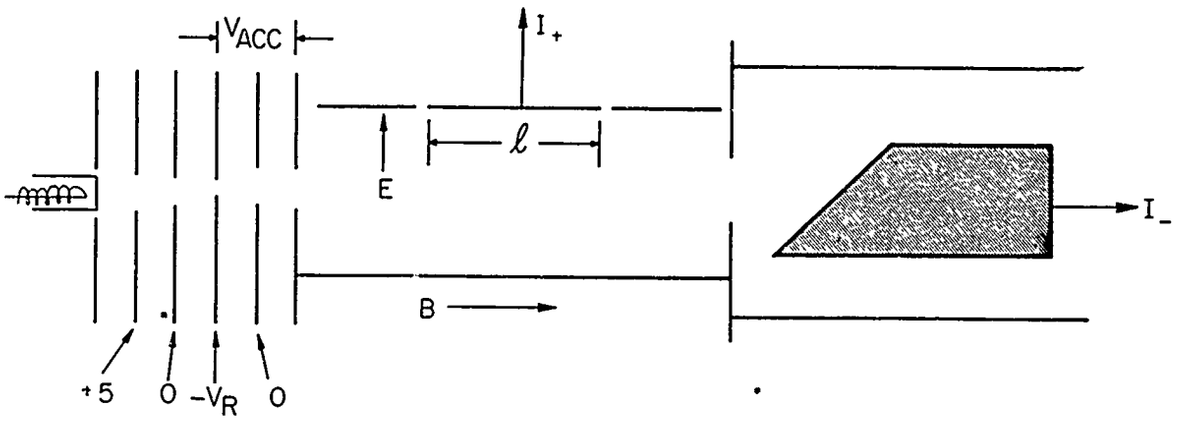

FIG. 13 Cross section apparatus. The spacing between electrodes in the gun was 1 mm. The height of the aperture in the retarding electrode was 0.2 mm. The length of the ion collector was $\ell = 26.6$ mm . The size of the gaps between this collector and the guard plates is strongly exaggerated.

The potentials indicated below the gun in Fig. 13 are all with respect to the cathode. All voltages were supplied from batteries. The narrow-slit retarding electrode is at a potential $-V_R$. Only electrons with energies above V_R will enter the acceleration region and gain an energy V_{ACC} before entering the collision region between the parallel plates. A small change ΔV_R in the retarding potential gives a change ΔI_- in the electron current and a corresponding change ΔI_+ in the ion current. If only singly charged ions are produced, the cross section can be determined from the relation

$$\sigma = \frac{\Delta I_+}{\Delta I_-} \frac{1}{n\ell} , \tag{38}$$

where n is the cesium atom number density and ℓ is the length of the interaction region. The energy resolution obtained in this mode of operation is better than 0.1 eV, which is sufficient for studying threshold behavior and fine structure on the ionization curve. At higher energies where no fine structure prevails the high resolution of the RPD method is not needed. Therefore for energies above 30 eV we have maintained V_R constant and used the ratio I_+/I_- instead of $\Delta I_+/\Delta I_-$ in Eq. (38).

The potential of the electron collector was made sufficiently high to ensure saturation of electron current at all energies. The high electric field at the collector surface will also prevent secondary electrons from entering the collision region. The performance of the electron beam is demonstrated in Fig. 14. . After alignment in the magnetic field, the current is independent of energy to within $\pm$ 1/2 %. Typical electron currents used in this investigation were from 0.1 - 1 μA .

The ions produced between the parallel plates initially have zero kinetic energy and will move to the upper plates in a proper $\underline{E} \times \underline{B}$ field configuration. The guard plates on either side of the ion collector establish a uniform electric field $\underline{E}$ and accurately define the length ℓ of the collision region. The ion trajectories are cycloidal, with drift in the direction of $\underline{E} \times \underline{B}$ and height

$$h = \frac{2M|\underline{E}|}{Ze|\underline{B}|^2} , \tag{39}$$

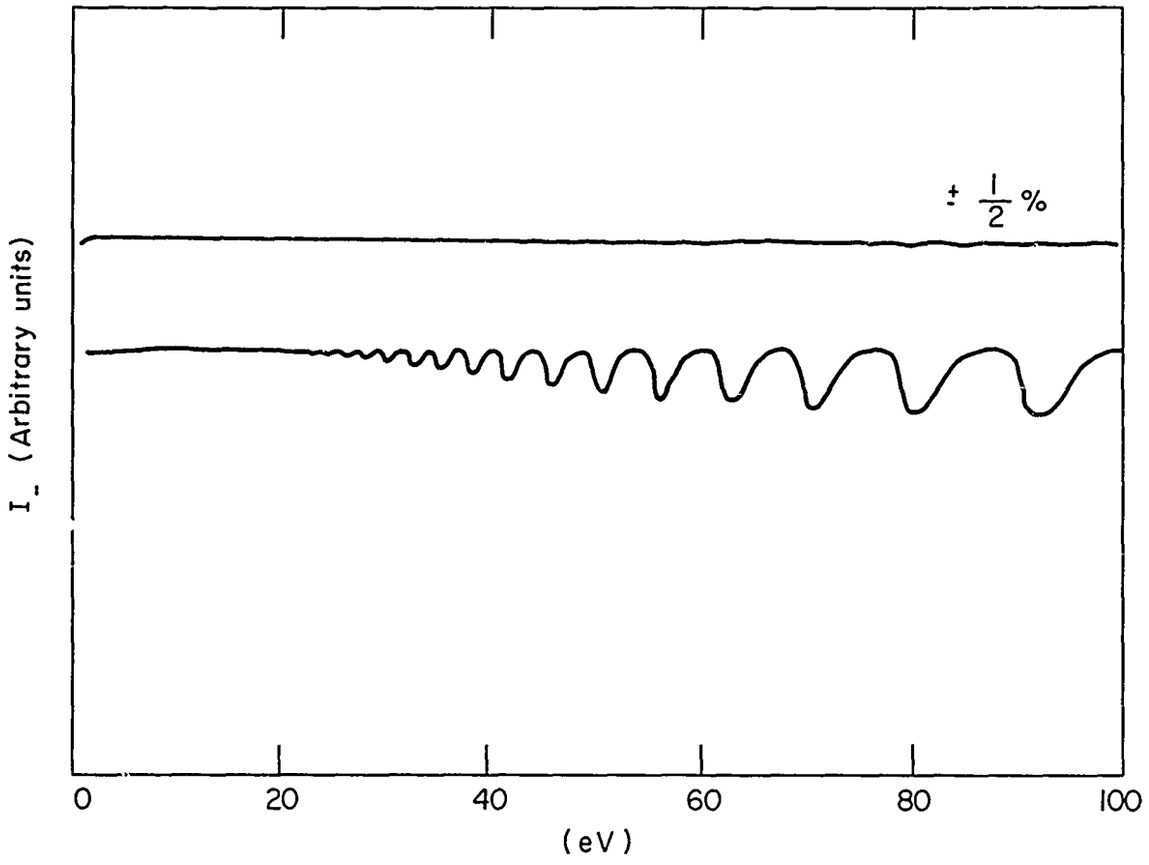

FIG. 14 Electron current I_- as a function of energy before (lower curve) and after elignment (upper curve) in the magnetic field. B = 500 Gauss.

where e is the electronic charge and M and Z are the ionic mass and charge number, respectively. As long as half of the parallel-plate separation is less than h (i.e., $\frac{d}{2} < h$) for $Z = Z_{max} = 3$, complete collection of all ionic species is assured. This requirement was always satisfied in the experiment.

The actual measurement of the ion current I_+ is complicated by cesium deposited on all insulator surfaces, thereby forming a leakage path for the current. By using ceramic insulators and a guard ring around the ion collector feedthrough, we were able to maintain the leakage resistance of this part above 10 MΩ . This is a factor of 100 - 1000 higher than the effective input impedance of the Keithley 610 B which was used for the measurement of the ion current.

4.2.3 Surface Ionization Detector - When the mean free path of the atoms is much larger than characteristic dimensions of the apparatus, Knudsen flow can be assumed and the density $n(T)$ in the interaction region at the temperature T can be found from

$$n(T) = N_0 \frac{T_0}{\sqrt{T_{Cs} T}} p(T_{Cs}) \quad . \tag{40}$$

Here N_0 is the gas number density at 1 torr at $T_0 = 273^0K$ and $p(T_{Cs})$ is the vapor pressure at the surface of the reservoir which has temperature T_{Cs} . Since $n(T) \propto T^{-\frac{1}{2}}$, it is more than sufficient to keep the temperature T in the collision region constant to within $\pm 5^0K$. On the other hand, the strong dependence of the vapor pressure on temperature requires that T_{Cs} be constant within $\pm 0.05^0K$. (A temperature change $\Delta T_{Cs} = 0.1^0$ corresponds to $\Delta n/n \approx 1\%$.)

Experimentally, prudence must be exercised in the application of Eq. (40). First, Knudsen, or molecular flow can only be established when all surfaces are covered with cesium.[27] Some workers[28,29] have reported that this might take many days, especially at surfaces where absorption of atoms will obstruct the specular reflection of atoms that is required in Knudsen's theory. Secondly, there exists in the literature disagreement on the values of the cesium vapor pressure in the range of our experiment.

By comparison we find that the recommended values of Honig[30] and of Hultgren et al.[31] are 20 - 30% below Nesmeyanov's[32] average values and Taylor and Langmuir's[25] formulas. Recently, Rozwadowsky and Lipworth[33] made optical absorption measurements of the density of saturated cesium vapor and obtained results in excellent agreement with those of Taylor and Langmuir.[34] Consequently, we have decided to use the latter values and complement these with our own surface ionization detector measurements.

The construction of the surface ionization detector (SID) is shown in Fig. 15. Above the center of a guarded circular copper plate a hot tungsten wire is stretched parallel to the surface. Positive ions produced over the length D are collected on the central part of the ion collector and give a current

$$I_{SID} = \frac{e}{4} n \langle c \rangle F , \qquad (41)$$

where $\langle c \rangle$ is the average thermal velocity of the cesium atoms and $F = \pi d_w D$. By comparison with another SID with a rectangular collector, we found that all ions generated over the circular collector were measured.

The tungsten wire was aged according to the recommended procedure of Taylor and Langmuir.[24] It was first heated to 2400°K for 24 hours, the temperature was then increased to 2600°K for a period of 1 hour, and finally the wire was given 4 - 6 short flashes at 2900°K. The filament temperatures were determined from the tables of Jones and Langmuir.[34] When tungsten filaments were treated in this way at background pressures of 10^{-9} to 10^{-8} torr, we found, from X-ray diffraction analysis, a layer of tungsten carbide on the surface. The carbon probably comes from impurities in the volume of the material. Suppliers of tungsten give the information that all wires contain some carbon, at least 10 - 15 ppm, because of the fabrication procedure. From measurement of the electron emission as a function of filament temperature we found the work function to be about 5.6 volts, which is sufficiently high to ensure ionization of cesium atoms. When the high-temperature aging took place at much higher pressures (10^{-4} - 10^{-5} torr), the X-ray diffraction did not reveal any carbides at all. The explanation of this is probably that carbon at the surface reacts with oxygen to give CO.

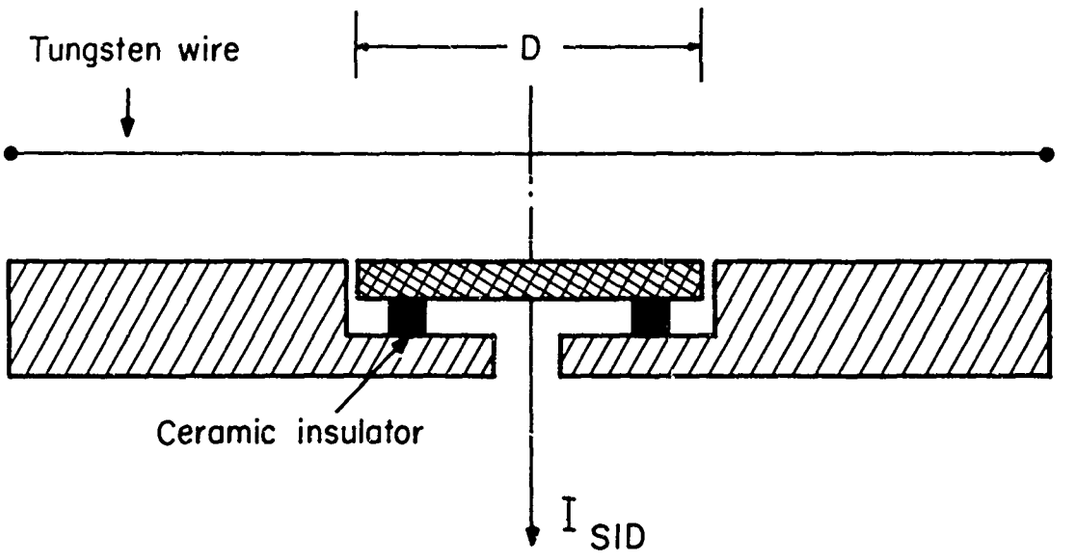

FIG. 15 Surface ionization detector. The diameter of the wolfram wire was $d_W = 1.28 \times 10^{-2}$ cm. D = 2.44 cm.

Nevertheless, both surfaces with and without carbides gave the same cesium densities when used in surface ionization detectors.

Absolute measurements of the density of cesium atoms in the vapor phase by means of surface ionization are based on the observation of Langmuir and Kingdon[35] that all atoms leave the surface as ions. (The use of hot wires for density determinations in atomic beams has been studied and discussed by Datz and Taylor[36] and McFarland and Kinney.[37]) By using Eq. (41) for determination of the density we found values that agree with those calculated from Taylor and Langmuir's formulas[25] to within $\pm$ 3%. A basic requirement for this agreement to occur is that the whole apparatus be in thermodynamic equilibrium with the cesium reservoir. This condition was reached about two weeks after cesium was introduced into the system. The distance between the cesium pool and the top of the tube (about 1 meter) combined with the time it takes to cover all surfaces with cesium accounts for part of the delay. In practice we found that the density increased very slowly as the equilibrium condition was approached.

4.2.4 Consistency Checks - Some of the precautions that must be made in electron beam ionization experiments have been discussed by Briglia and Rapp.[38] First, from Eq. (38) we would expect to find the saturated ion current proportional to the saturated electron current. In cesium this was verified for $0.1 \leq I_- \leq 10$ μA. (A test case in helium gave $I_+ \propto I_-$ for $10^{-10} \leq I_- \leq 10^{-5}$ A.) The collection efficiencies for electrons and ions have already been discussed in Section 4.2.2.

Furthermore, proportionality between I_+ and cesium density was found over the density range $5 \times 10^{10} \leq n \leq 10^{12} cm^{-3}$. At the highest density of $10^{12} cm^{-3}$ the electron mean free path is $\Lambda = (n\sigma)^{-1} \approx (10^{12} \times 10^{-15})^{-1} = 10^3 cm$, which is much longer than the length ℓ of the interaction region in Fig. 13. Therefore, even at the highest density used, the probability of one electron producing more than one ionization event is extremely small.

Beam electrons with perpendicular velocity components will travel in helices parallel to the magnetic field. The path length along one particular helix is, of course, larger than the length ℓ as defined in

Fig. 13. The correction formula presented by Massey and Burhop[39] is inapplicable to most practical guns, as pointed out by Asundi.[40] The electric lens configuration[41] in our electron gun tends to minimize angular spread in the beam. Since the increase in path depends strongly on the magnetic field, the best way to check the constancy of the ionization length is to measure I_+/I_- as a function of B , keeping all voltages constant. We found I_+/I_- to be constant for the range of parameters used in the experiment.

Finally we checked that the current of stray electrons to the entrance and exit electrodes in the ionization region and to the lower parallel plate was 1000 times smaller than the beam current. Stray electrons were not detected on the ion collector.

The energy scale was calibrated by letting helium into the tube together with the cesium and measuring the resonance[42] in the elastic scattering cross section at 19.3 eV. The resonance shows up as an increase in transmitted electron current. The other point on the energy scale was taken at the appearance of Cs^+ ions at 3.89 eV. In addition, we plotted the electron beam current as a function of energy and extrapolated the current to zero[38] to find the contact potential difference between the collision region and the retarding electrode. The measured voltage difference between the retarding electrode and the collision region includes the contact potential difference in the tube as well as contributions from the leads between the tube and the voltmeter. This total correction was 0.8 V, independent of method of measurement. When a system is immersed in a vapor, all surfaces will be automatically covered with atoms from the vapor, thereby providing areas of constant contact potential. For this reason we believe that the true contact potential difference in the tube is much smaller than the measured value of 0.8 V.

The spread in energy in the electron beam can be attributed to thermal spread as the electrons leave the cathode surface and to non-uniform distribution of contact potential on electrode surfaces. If the cathode temperature is T_c , the average energy of the emitted electrons is $2kT_c$. The Philips impregnated cathode in our electron gun was operated at temperatures of about 800^0K, corresponding to an average thermal energy of 0.14 eV. We obtained information about the spread in electron energy

by (1) measuring the tailing in ion current and by (2) retarding potential measurement of the current to the electron collector. The tailing in ion current at threshold indicated an energy spread of 0.05 eV. From the latter method we found a spread in energy (defined as the full half-width of the differentiated current-voltage curve) of less than 0.1 eV. This spread was independent of the beam energy.

4.3 Results and Discussion

4.3.1 Data Analysis - The ion current that is measured on the collector of our total ionization apparatus is

$$I^{+}_{tot} = I(Cs^{+}) + I(Cs^{++}) + I(Cs^{+++}) + \ldots , \tag{43}$$

where the current of Cs^{n+} ions is

$$I(Cs^{n+}) = I_{-} \, n\ell\sigma(Cs^{n+}) . \tag{44}$$

We determine the current of singly ionized atoms by multiplying the total ion current with the ratio

$$R = I(Cs^{+})/I^{+}_{tot} .$$

This ratio is identical with the correction factor $[\Sigma n\alpha_n]^{-1}$ used by Brink,[19] where

$$\alpha_n = \sigma(Cs^{n+})/\sigma(Cs^{+}) .$$

From a careful analysis of Tate and Smith's paper,[18] we obtain the current ratio shown in Fig. 16. According to Tate and Smith the ionization curve for Cs^{+} might be 15% too low due to incomplete collection of ions. It should be noted that the Tate and Smith ordinates as presented in their paper can be interpreted in different ways. They mention expressions such as "likelihood of ionization", "probability of ionization", and "efficiency of ionization", without really defining any of these. They claim the ratio of the different ion currents to the electron current gives "a measure of the relative probability of the production of the different ions." As will be shown later, different interpretations will give different results for the Cs^{+} cross section.

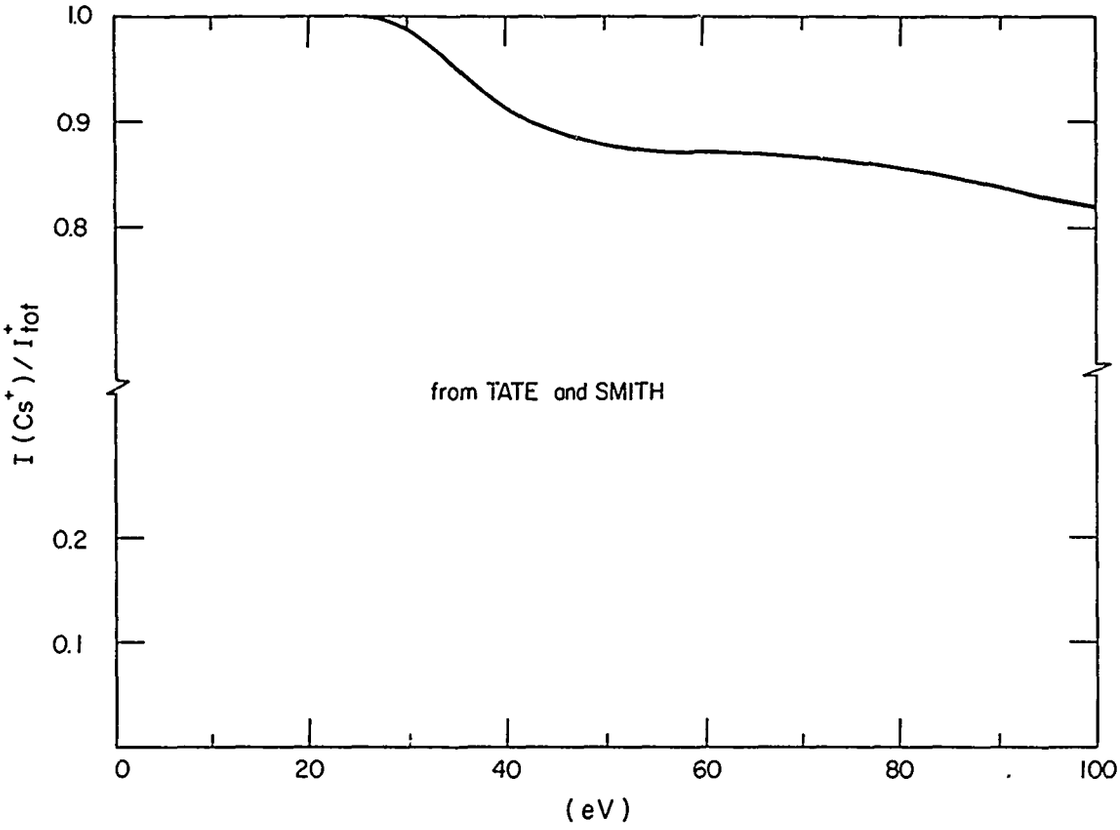

FIG. 16 $I(Cs^+)/I^+_{tot}$ as a function of electron energy as obtained from Tate and Smith (ref. 18).

4.3.2 Compilation of Results - Absolute data for the Cs^+ cross section as a function of electron energy are shown in Fig. 17. The curve in the middle represents the present measurements. The measurements for all curves were performed in systems in which cesium vapor was in supposed thermodynamic equilibrium with a liquid-phase reservoir. Korchevoi and Przonski[22] used the cylindrical collector arrangement developed by Schulz,[43] whereas Heil and Scott[21] modified the Tate and Smith-type apparatus by depositing the ion collector and guard ring on the inside of a glass tube. The points represent crossed-beam experiments by Brink[19] and by McFarland and Kinney.[20] If McFarland and Kinney take the Tate and Smith ordinates as probabilities of ionization, they get the filled circles as values for the cross section. On the other hand, if the Tate and Smith ordinates are interpreted as ion currents proportional to $n\sigma(Cs^{n+})$, the higher values indicated by the open circles[45] are obtained. No energy values have been assigned to the maximum cross sections reported by Brink[19] and by McFarland and Kinney.[20] From the shape of the cross section curves we see that a rather flat maximum occurs at 28 eV. Accordingly the points from the crossed-beam experiments have been plotted at this energy. At the maximum cross section (filled circle at 28 eV) the probability of ionization is approximately equal to $I(Cs^+)/I_-$, since very few Cs^{++} ions are produced at this energy. The McFarland and Kinney value at maximum is therefore insensitive to interpretation of the Tate and Smith paper.

Our results seem to coincide with those of Korchevoi and Przonski for energies up to about 10 eV. Differences in initial slope are not discernible because of the scale used in Fig. 17. (The threshold region of the cross section will be discussed in a separate paragraph.)

It is interesting to normalize the curve of Tate and Smith to ours at 28 eV and compare the shape of the cross section curves. The total ion current I^+_{tot} as reported by Tate and Smith and remeasured here falls off almost linearly by 1/2 % per eV from 28 to 100 eV. Since we are using the ratio of $I(Cs^+)/I^+_{tot}$ from Tate and Smith, it is not surprising to find good agreement in this energy range. Most apparent is the minimum at about 19 eV which is 13% below the maximum on the Tate and Smith curve and 17% below on ours. In the Heil and Scott work, the "dip" on the curve is about 10% of the maximum. We have found that this dip decreases with increasing

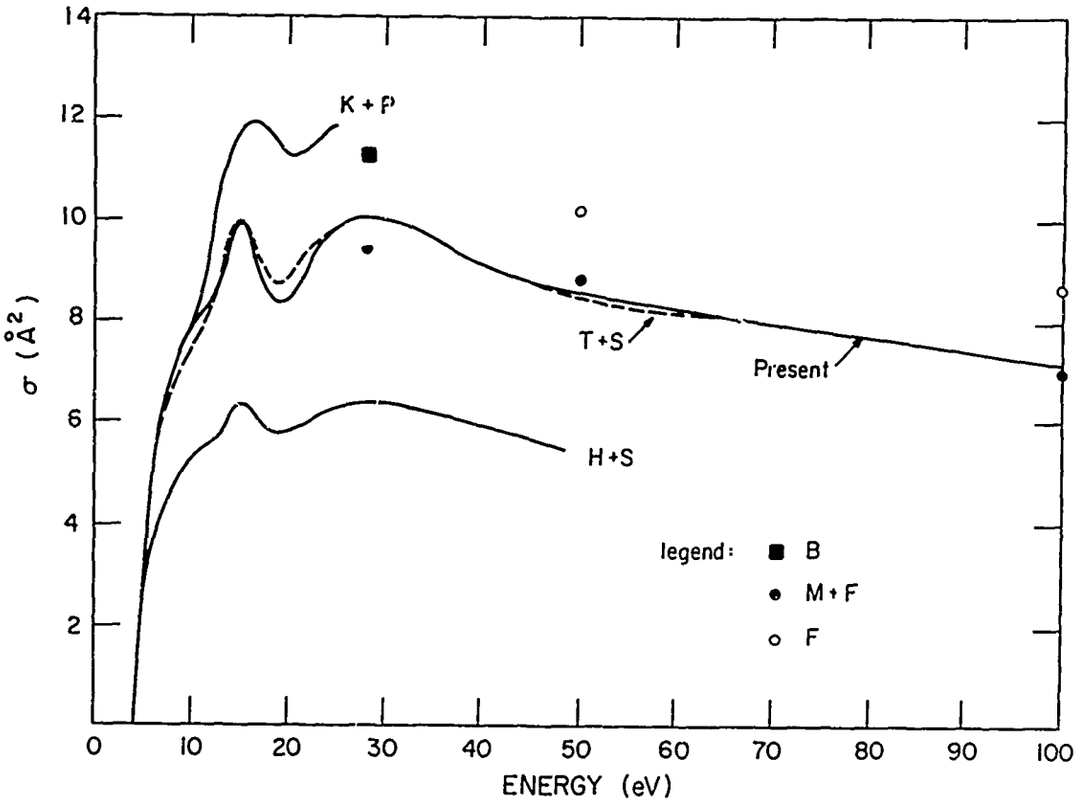

FIG. 17 Ionization cross section for Cs^+ vs electron energy. The fulldrawn curve extending to 100 eV represents the present measurements.
Legend: H+S: Heil and Scott (ref. 21).
K + P: Korchevoi and Przonski (ref. 22).
B: Brink (ref. 20).
M + K: McFarland and Kinney (ref. 20).
M: McFarland (ref. 45).
T + S: Relative measurements of Tate and Smith (ref. 18) normalized to the present maximum at 28 eV.

electron current, presumably because higher currents result in a larger spread in energy.

Part of the disagreement between the various results can be understood by analyzing the experimental techniques. Since Korchevoi and Przonski had no guard rings outside their ion collector, the effective length of the collision region is larger than ℓ. The cross section is inversely proportional to ℓ, which might explain why the results of Korchevoi and Przonski are higher than those of other workers.

The lowest cross section values have been obtained by Heil and Scott. There might have been a systematic error in the determination of the cesium density, as discussed by McFarland,[45] or the apparatus might not have been in complete thermodynamic equilibrium.

Basic difficulties in crossed-beam experiments are the measurements of the cesium atom density and the determination of the interaction volume. Brink[19] and McFarland and Kinney[20] were using two different experimental systems with different geometry factors. In spite of complicated calibration procedures the results agree within the experimental uncertainties, which lends confidence to the reliability of this type of experiment. One great advantage of the crossed-beam experiment is that insulators can be protected from the cesium flux, thereby eliminating the leakage current problem prevailing in vapor-phase systems.

The accuracy of the present data is 7%, based upon the following estimates:

$$\frac{\Delta I_+}{I_+} = 5\%; \qquad \Delta I_-/I_- = 3\%;$$

$$\Delta n/n = 3\%; \text{ and } \Delta\ell/\ell = 2\% .$$

However, the high energy part of the curve might be too low due to a systematic error in the correction factor $I(Cs^+)/I^+_{tot}$. The maximum systematic error in the work of Tate and Smith is 15% but this error might be energy dependent. Since McFarland[45] and Heil and Scott[21] have been using the same

correction factor, this systematic error is also inherent in their results. Korchevoi and Przonski[22] avoided this ambiguity by limiting their measurements to the range below the second ionization potential.

By taking the average of the results of all authors, at maximum we obtain a value of 9.8 $\mathring{A}^2$. It has been assumed here that the curve of Korchevoi and Przonski extrapolates to 12 $\mathring{A}^2$ at 28 eV.

4.3.3 Ionization Mechanisms

The shape of the ionization cross section curve in cesium is determined mainly by the cross section for removal of the 6s electron. According to Geltman,[46] the cross section close to threshold (3.89 eV) is expected to increase in proportion to the electron energy in excess of the ionization energy. In electrical discharges, atoms are ionized by the electrons on the "tail" of the electron energy distribution, and for this reason it is important to know the initial slope of the cross section. Data for this quantity as well as the range of linearity are shown in Table V.

Table V. Threshold behavior of ionization cross section.

Author(s)	Slope ($\mathring{A}^2$/eV)	Range of linearity above threshold (eV)
Present work	2.7	≈ 1
Heil and Scott[a]	2.2	0.8
Korchevoi and Przonski[b]	1.7	unknown
Nottingham[c]	5.7	≈ 1.5

[a] Ref. 21. [b] Ref. 22. [c] Ref. 47.

The measurement of Nottingham[47] was made in an electrical discharge where accurate knowledge of the parameters needed to determine the cross section is difficult to establish. It is surprising to observe that Korchevoi and Pronzski, who reported the highest maximum cross section among the workers quoted here, obtained the lowest value of the slope at 1.7 $\mathring{A}^2$/eV. Since they do not state the range of linearity, there is a slight possibility that their

number refers to the tailing part of the ionization curve due to insufficient energy resolution. It has been mentioned already that the maximum of our cross section agrees closely with the results of the crossed-beam experiments, and for this reason we recommend our value of 2.7 $\mathring{A}^2$/eV for the slope.

As a first attempt to explain the structure (including the two maxima) of the cross-section curve, we have calculated the partial cross sections for removal of 6s, 5p, and 5s electrons using the Gryzinsky[48] formula (Fig. 17). The total cross section resulting from the sum of the partial Gryzinsky cross sections agrees very closely with the present experimental results. However, the most conspicuous difference is that the "dip" on the Gryzinsky curve is only 1% of the maximum, whereas a value of 17% was found here. We therefore conclude that ionization of core electrons is not capable of explaining the structure of the ionization curve, and that additional mechanisms are needed. Similar types of structure have also been observed on the ionization curves of Rb^+ [18, 19] K^+ [18,19,49] and Mg^+ [49], but in the following we shall restrict our discussion to Cs^+. Heil and Scott have suggested that the first peak is due to autoionization and the second due to production of excited ions. The Gryzinsky calculation shows that the cross section for ionization of one of the 6p electrons is about 0.5 $\mathring{A}^2$, and for this reason the production of excited ions seems likely.

A value of 1 $\mathring{A}^2$ has been estimated by Heil and Scott for excitation of the autoionization level. Our data imply a value of about 1.6 $\mathring{A}^2$ if the first peak is attributed to autoionization. Interpreting the first peak in this way implies the existence of a doublet autoionization level (spin = 1/2) at about 12 eV above the Cs^+ ground state. Feldman and Novick[50] have observed a quartet (spin = 3/2) autoionization level at 12.6 $\pm$ 0.3 eV. Their state is metastable (with lifetime about 40 μsec) because it cannot make a dipole transition to the singlet (spin = 0) continuum states. However, the presence of a quartet state at this energy strongly suggests that there is also a doublet state very near in energy, for instance the $6p^5 6s^2$ electron configuration observed by Beutler and Guggenheimer.[51] Therefore, attributing the first peak to autoionization is probably justified.

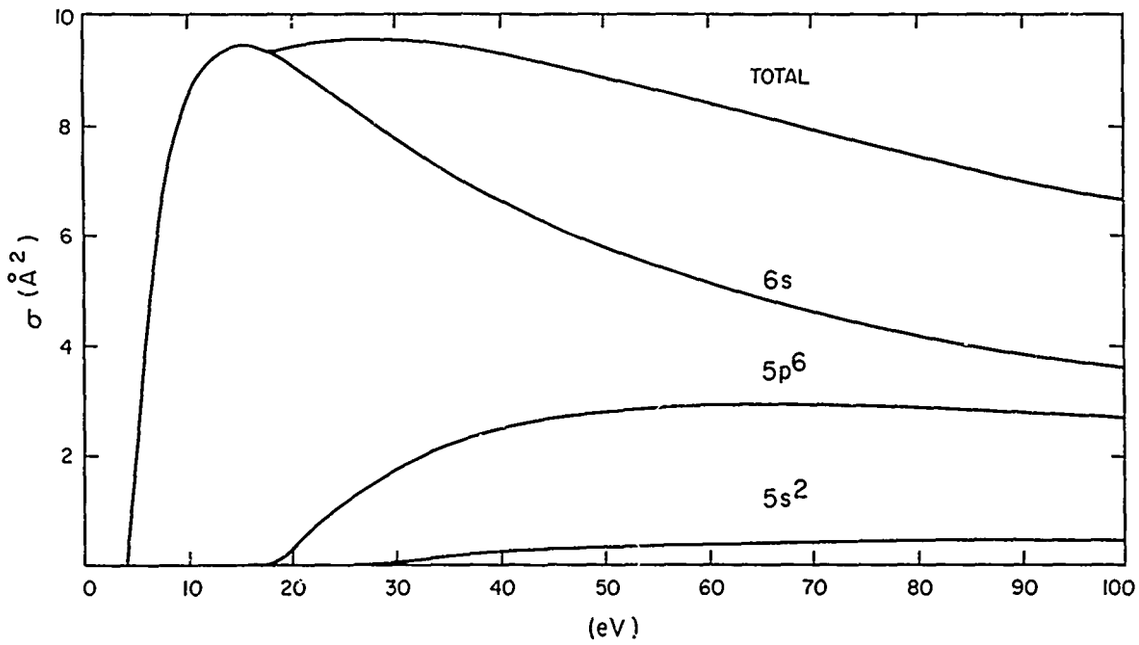

FIG. 18 Gryzinsky calculation of the cross section. Following McFarland (ref. 46), threshold values of 3.89, 17.2, and 26 eV were used for removal of 6s, 5p, and 5s electrons, respectively.

The cross section for excitation of the doublet autoionization level is expected to be larger than for excitation of the quartet metastable level as the latter requires a spin change of the 5p core electron of the cesium atom. This is consistent with Feldman and Novick's values of the cross section as 10^{-2} - 10^{-3} $\mathring{A}^2$ for quartet excitations and our observation of about 1.6 $\mathring{A}^2$ for the doublet excitation. The lifetime of the doublet state is too short to be observed in the time-of-flight type experiment of Feldman and Novick.

In conclusion, it should be pointed out that the ionization mechanisms of the cesium atom are not completely understood. Experimentally, one can get information about autoionization by studying the kinetic energy (12.6 - 3.9 = 8.7 eV) of the electron ejected from the autoionizing level. This will be the objective of another investigation.

5.0 REFERENCES

1. R. H. Curry, D. W. Norcross and P. M. Stone, Annual Report No. 1, Contract Nonr 5154(00), ONR (1967).

2. D. W. Norcross and P. M. Stone, J. Quant. Spectrosc. Radiat. Trans. , (to be published) SRRC-RR-67-22.

3. D. W. Norcross and P. M. Stone, J. Quant. Spectrosc. Radiat. Trans. , 6, 277 (1966).

4. W. H. Reichelt, Int'l Conf. on Thermionic Electrical Power Generation, London, 1965.

5. T. Holstein, Phys. Rev. 83, 1159 (1951).

6. W. L. Nighan, Proceedings of Thermionic Conversion Specialist Conference, Houston, Texas, 1966.

7. D. R. Wilkins and E. P. Gyftopoulous, J. Appl. Phys. 37, 3533 (1966).

8. J. M. Houston, Report on XXIV Annual Conference on Physical Electronics, Cambridge, Massachusetts, 1964, p. 211.

9. Y. Lee and B. H. Mahan, J. Chem. Phys. 43, 2016 (1965).

10. D. W. Norcross, Report on XXVII Annual Conference on Physical Electronics, Cambridge, Massachusetts, 1967. Copy attached as Appendix to this Report.

11. L. Agnew, Report of Thermionic Conversion Specialist Conference, San Diego, California, 1965, p. 119.

12. L. Agnew and C. Summers, Proceedings of VII Int'l Conference on Phenomena in Ionized Gases, Belgrade, 1965. Vol. II, p. 574.

13. F. L. Mohler, J. Res. Nat. Bur. Standards 10. 771 (1936). 17, 849 (1936).

14. P. M. Stone and L. Agnew, Phys. Rev. 127, 1157 (1962).

15. H. R. Griem, Phys. Rev. 128, 515 (1962).

16. L. I. Grechikhin, Optics and Spectroscopy 22, 301 (1967).

17. H. R. Kratz, Phys. Rev. 75, 1844 (1949).

18. J. T. Tate and P. T. Smith, Phys. Rev. 46, 773 (1934).

19. G. O. Brink, Phys. Rev. 127, 1204 (1962).

20. R. H. McFarland and J. D. Kinney, Phys. Rev. 137, A1058 (1965).

21. H. Heil and B. Scott, Phys. Rev. 145, 279 (1966).

22. Yu. P. Korchevoi and A. M. Przonski, Soviet Phys.-JETP 24, 1089 (1967).

23. R. E. Fox, W. M. Hickam, D. J. Grove and T. Kjeldaas, Jr., Rev. Sci. Instr. 26, 1101 (1955).

24. J. B. Taylor and I. Langmuir, Phys. Rev. 44, 423 (1933).

25. J. B. Taylor and I. Langmuir, Phys. Rev. 51, 753 (1937).

26. Cesium impurities of consequence in this experiment are: Na - 5 ppm, Rb - 2 ppm, and K - 1 ppm.

27. P. Clausing, Ann. Physik 7, 489 (1930).

28. K. Hoffmann, Exp. Technik der Physik 10, 419 (1962).

29. F. Kirchner, Z. angew. Physik 11, 167 (1959).

30. R. E. Honig, RCA Review 23, 567 (1962).

31. R. Hultgren, R. L. Orr, P. D. Anderson, and K. K. Kelly, Selected Values for the Thermodynamic Properties of Metals and Alloys, (John Wiley and Sons, Inc., New York, London, 1963) p. 87.

32. A. N. Nesmeyanov, Vapor Pressure of the Chemical Elements, edited by R. Gary, (Elsevier Publishing Company, Amsterdam, London, New York, 1963) pp. 146-150.

33. M. Rozwadowski and E. Lipworth, J. Chem. Phys. 43, 2347 (1965).

34. H. A. Jones and I. Langmuir, General Electric Review 30, 310 (1927).

35. I. Langmuir and K. H. Kingdon, Proc. Roy. Soc. (London) 107, 61 (1925).

36. S. Datz and E. H. Taylor, J. Chem. Phys. 25, 389 (1956).

37. R. H. McFarland and J. D. Kinney, Proceedings of the Seventh Int'l. Conf. on Phenomena in Ionized Gases, Vol. 1, (Belgrad 1966) p. 254.

38. D. D. Briglia and D. Rapp, J. Chem. Phys. 42, 3201 (1965).

39. H.S.W. Massey and E.H.S. Burhop, Electronic and Ionic Impact Phenomena (Oxford University Press, 1952) p. 34.

40. R. K. Asundi, Proc. Phys. Soc. 82, 372 (1963). (There is a misprint in the first equation in this paper.)

41. J. R. Pierce, Theory and Design of Electron Beams (D. van Nostrand Company, Inc., 1954, 2nd Edition) pp. 96-101.

42. C. E. Kuyatt, J. A. Simpson, and S. R. Mielczarek, Phys. Rev. 138, A385 (1965).

43. G. J. Schulz, Phys. Rev. 112, 150 (1967); J. Chem. Phys. 33, 1661 (1960).

44. R. H. McFarland, Phys. Rev. 139, A40 (1965).

45. R. H. McFarland, Phys. Rev. 159, 20 (1967).

46. S. Geltman, Phys. Rev. 102, 171 (1956).

47. W. B. Nottingham, Advanced Energy Conversion 3, 245 (1963).

48. M. Gryzinsky in Atomic Collision Processes, edited by M.R.C. McDowell (North-Holland Publishing Company, Amsterdam, 1964), pp. 226-236. (Notice that the value of σ_0 in Eq. (4) of this reference is a factor of 100 too low.)

49. Y. Kaneko, J. Phys. Soc. Japan 16, 2288 (1961).

50. P. Feldman and R. Novick, Phys. Rev. 160, 143 (1967).

51. H. Beutler and K.Guggenheimer, Z. Physik 88, 25 (1934).

APPENDIX I

DEPARTURE FROM LTE IN THE THERMIONIC CONVERTER

by

D. W. Norcross

(Published in Report on Twenty-Seventh Annual Conference, Physical Electronics, Cambridge, Massachusetts, 1967, pp. 332-340, and as SRRC-RR-67-19.)

DEPARTURE FROM LTE IN THE THERMIONIC CONVERTER*

D. W. Norcross (introduced by P. M. Stone)
Sperry Rand Research Center
Sudbury, Massachusetts

Abstract

Reported electron temperature and density profiles across the interelectrode space of a thermionic converter[1] have been analyzed using a model which has been described previously.[2] For each set of T_e and N_e points, effective coefficients for ionization and for radiative energy loss are computed. These coefficients and the neutral density (obtained through the assumption of a linear heavy-particle temperature distribution across the gap, and the ideal gas law) yield the rates for net ion production and radiative energy loss from all sources except the resonance lines. Energy loss from resonance lines and the ion production cost are considered separately. The following general conclusions can be drawn from the consistent behavior of the results: i) the area within 0.4 mm of the emitter is a source of ion-electron pairs, the rest of the plasma being a sink; ii) inelastic energy losses decrease monotonically from the emitter to the collector; iii) these effects are relatively independent of cesium pressure, but are generally proportional to output current density.

Introduction

Future progress in the effort to understand the operation of the cesium filled thermionic converter would seem to depend heavily on obtaining an accurate solution to the equations governing the transport of particles and energy across the interelectrode plasma. Two of the most important terms in these equations are the rates for production or loss of ion-electron pairs, and the rate of loss of electron kinetic energy either directly through ionization of neutral atoms or indirectly through escape of radiation from the volume of the plasma.

A model has been developed which yields these rates if the following information is given: N_e and T_e profiles across the plasma, electrode temperatures and spacing, plasma thickness, and cesium pressure. The model incorporates the assumptions that the plasma is radially homogeneous; that the only species present are ions, electrons and neutral atoms; that mean-free-paths for electron-atom collisions are small compared to plasma dimensions; that gradients in T_e and N_e are negligible in distances comparable to these mean-free-paths; that the electron velocity distribution is Maxwellian; and finally that the plasma is optically thin to all but resonance radiation.

The model consists of an equation for the rate of change of the population of each atomic level due to inelastic electron-ion and electron-atom collisions, and spontaneous radiative decay and recombination. If certain criteria are satisfied, the excited

---

* This work was supported by the Office of Naval Research.

state populations can be assumed constant in time, and the rate of change of electron density equals the rate of change of ground state density. The equations can then be solved for the excited state populations in terms of the ground state density, and for the rates of electron-ion pair production and radiative energy loss. Since the model has already been discussed,[2] the details of the solution will not be considered here. An exhaustive presentation will become available shortly.[3]

The Model

Application of the model to a given set of values of N_e and T_e yields results which can be expressed by the two equations

$$-dN_e/dt = \alpha N_e^3 - SN_eN_1 \quad cm^{-3}sec^{-1} \tag{1}$$

$$-dR_1/dt = AN_e^2 + BN_1 \quad watt\ cm^{-3} \tag{2}$$

where $-dN_e/dt$ is the rate of loss of ion-electron pairs, $-dR_1/dt$ is the rate of loss of radiative energy from all but the resonance lines, and N_1 is the density of ground state atoms. The coefficient α can be interpreted as an effective three-body collisional-radiative recombination coefficient, and S can be interpreted as an effective ionization coefficient. The coefficients A and B do not have such a simple physical interpretation. These four coefficients are functions of N_e and T_e only.

It should be clearly understood that even though the electron density at any point in the plasma volume is constant, the rate given by Eq. (1) is not necessarily zero. This rate is due to atomic processes only and must be balanced by macroscopic processes such as diffusion. It should also be noted that Eq. (2) represents the total electron kinetic energy loss only when Eq. (1) is zero. For non-zero $-dN_e/dt$ there is an additional energy loss term

$$-dR_2/dt = 6.22 \times 10^{-19}\ dN_e/dt \quad watt\ cm^{-3} \tag{3}$$

which represents a cost of 3.89 eV per ion-electron pair produced.

Finally (as was pointed out by Kniazzeh in the discussion period), while it may be correct to assume that resonance radiation is completely trapped in solving for the coefficients in Eqs. (1) and (2), the very small fraction of the resonance radiation which does escape may be a significant energy loss. For typical conditions the Doppler and pressure contributions to the line half-width are comparable, but since the line center is completely reabsorbed, it is the line wings which determine the amount of radiation escaping, and hence only the pressure broadening need be considered.[4] For pressure broadened lines in homogeneous plasmas, Holstein gives the following formulae for the fraction of radiation (g) which escapes[5]

$$g_p = 1.333(\pi k_p L)^{-1/2} \tag{4}$$

$$g_c = 1.376(\pi k_p R)^{-1/2} \tag{5}$$

for plane parallel and cylindrical geometries of thickness L and radius R, respectively. The constant k_p is the absorption coefficient at the center of the line given by[†]

$$k_p = \frac{4\pi}{1.92}\left(\frac{\omega_U}{\omega_L}\right)^{1/2} \lambda_o^{-1} \tag{6}$$

The statistical weights of the emitting and absorbing state are ω_U and ω_L, respectively. For the first resonance line of cesium (the doublet having been coalesced into a single level), Eqs. (4) and (5) give $g_p = 2.074 \times 10^{-3}\, L^{-1/2}$ and $g_c = 2.141 \times 10^{-3}\, R^{-1/2}$, where L and R are in cm. Clearly, for spacings greater than 0.05 cm more than 99% of the resonance radiation is trapped. It should be noted that this result is dependent on particle pressures or temperatures only to the extent that pressure broadening must dominate in the wings of the line.

The transition probability of the 6P state is $3.57 \times 10^7 \text{sec}^{-1}$, and hence an approximate expression for the power loss from the resonance lines in a cesium plasma with cylindrical geometry is

$$-dR_3/dt = 1.72 \times 10^{-14} N_2(\epsilon L^{-1/2} + R^{-1/2}) \quad \text{watt cm}^{-3} \tag{7}$$

where N_2 is the 6P population cm^{-3} and ϵ is the emissivity of the electrodes. The contribution from higher resonance lines can safely be ignored in most cases because of the much lower density of these levels.

Solutions of the set of rate equations yielding the rate coefficients in Eqs. (1) and (2) show that for $N_e > 10^{13}$ and $g_2 < 10^{-2}$, complete resonance trapping can be assumed without introducing significant error.[2] Accordingly, complete sets of the coefficients α, S, A, and B were computed with $g = 0$. These results were seen to fit exponential curves of the type

$$\alpha = \alpha_o \exp\left[E_1/(kT_e)^{1/2}\right] \tag{8a}$$

$$S = S_o \exp\left[-E_2/kT_e\right] \tag{8b}$$

$$A = A_o \exp\left[E_3/(kT_e)^{1/2}\right] \tag{8c}$$

$$B = B_o \exp\left[-E_4/kT_e\right] \tag{8d}$$

[†] The numerical constant in Eq. (8) of Ref. 4 should be 1.92 instead of 2.74.[6]

where α_o, etc. and E_1, etc. are constants which are dependent only on N_e. Using Eqs. (8) and interpolating the tabulated values of α_o, etc. and E_1, etc. for a given N_e reproduces the results of the original calculation to within a few percent.

The degree of nonequilbrium predicted by the model is illustrated in Fig. 1, which is a plot of the results of Eq. (1) with $g = 0$ and $-dN_e/dt = 0$. The ground state density predicted by the model is plotted vs N_e for various values of T_e, along with that predicted by the Saha equation

$$N_1 = \left(\frac{2\pi\hbar^2}{mkT_e} \right)^{3/2} N_e^2 \exp (E_1/kT_e) \qquad (9)$$

where $E_1 = 3.89$ eV. The steady-state nonequilibrium calculation is seen to predict a higher value of N_1 for a given N_e, reflecting the effect of radiative decays in increasing the relative population of the lower bound levels. A more conventional, but equivalent, way of interpreting these plots is to consider that the model predicts a lower value of N_e for a given N_1 and T_e due to depletion of high bound levels and the continuum by radiative decay and recombination.

Application to Experiment

The model discussed above has been applied to experimentally obtained N_e and T_e profiles of Reichelt.[1] These data were taken in a thermionic diode operating in the ignited mode with an interelectrode spacing of 1 mm and an emitter-collector radius of 8 mm. The emitter and collector were tungsten and nickel, having emissivities of ~ 0.4 and 1.0, respectively, at their operating temperatures to radiation in the neighborhood of 8500 Å. Cesium pressures were above 1.9 torr. Spectroscopic measurements of T_e and N_e were taken at four points across the gap, each separated by approximately 0.2 mm, with a spatial resolution of ~ 0.1 mm. Thus each point is distinct from the adjacent points and over a volume of plasma which can be assumed homogeneous. The measured values of T_e and N_e ranged from 2000 to 2800°K and from 5×10^{13} to 5×10^{14} cm^{-3}, with an estimated experimental error of 5% and 10%, respectively.

At these operating conditions, the assumptions made in deriving Eqs. (8) are valid, and the trapping fractions are $g_p\bar{\epsilon} = 4.6 \times 10^{-3}$ and $g_c = 2.4 \times 10^{-3}$, implying that the assumption of $g = 0$ in calculating the coefficients in Eqs. (1) and (2) is also valid. Due to the high degree of resonance trapping, which forces the ground and first excited state into thermodynamic equilibrium at T_e,[2] Eq. (7) can be simplified to

$$-dR_3/dt = 1.72 \times 10^{-13} N_1 \exp(-1.432/kT_e) \quad \text{watt cm}^{-3} \qquad (10)$$

where kT_e is expressed in eV.

The experimental values of N_e and T_e were used to generate the coefficients α, S, A and B as in Eqs. (8). The ground state density N_1 was computed using the ideal gas law

$$P/k = N_eT_e + N_iT_i + N_aT_a \qquad (11)$$

The assumptions were made that the ion density $N_i = N_e$ and the ion temperature $T_i = T_a$, and that T_a varies linearly between the electrode temperatures. The total atom density N_a is related to N_1 by a simple partition function.

The results obtained for $-dN_e/dt$ are shown in Figs. 3 and 4. The emitter temperatures are given on the inset J-V curves. Several features are discernable: 1) the volume of the plasma within ~ 0.4 mm of the emitter appears to be a source of electron-ion pairs, while the rest of the plasma is a sink; 2) the production rate near the emitter is generally independent of pressure but 3) is generally proportional to the current for a given emitter temperature, and, 4) is generally inversely proportional to emitter temperature for a given current. Departures from these trends reflect departures in the corresponding relationships between T_e and output current J. The contribution to the electron current from the charged particle production of Figs. 3 and 4 is negligible. A production rate of $\sim 5 \times 10^{20} cm^{-3} sec^{-1}$ across the entire gap would be required to account for the measured current. On the other hand, the contribution to the ion current may be significant.

These conclusions must be highly qualified, since the sensitivity of $-dN_e/dt$ to T_e is great. For 39 of the 43 N_e-T_e sets analyzed, a change in T_e of less than 4% is sufficient to yield $-dN_e/dt = 0$. For the remaining points the required change in T_e was less than 10%. Hence, application of the model with $-dN_e/dt = 0$ in comparable systems can be expected to yield electron temperatures within experimental error for known values of N_1 and N_e. This approach has been used by Reichelt and others with Eq. (1) replaced by the Saha equation, with calculated values for T_e in good agreement with experiment. This is to be expected from the plots of Fig. 1 for $N_e > 5 \times 10^{13} cm^{-3}$.

Use of the Saha equation cannot, however, be assumed valid at lower plasma densities where departure from thermodynamic equilibrium is greater. The sensitivity of the model to the amount of resonance trapping increases quickly below $N_e = 10^{13} cm^{-3}$, so that the degree of nonequilibrium can be expected to be even greater than that shown in Fig. 1 for these densities.

The results obtained for $-dR_1/dt$ are shown in Figs. 4 and 5, which were calculated using the experimental values for T_e. The energy loss due to radiation from all but the resonance lines is seen to be generally proportional to current, but insensitive to changes in emitter temperature or pressure. The sensitivity to changes in T_e is not nearly as great as for $-dN_e/dt$ as is indicated by the error bars on one set of data, representing changes in T_e of 1% and 5%. The integrated total loss from this source is seen to be of the order of 1 watt.

Results for the energy loss associated with net ion production are not presented because of their strong dependence on T_e. It should be noted, however, that this may be a significant source of power loss, since a production rate of $10^{18} cm^{-3} sec^{-1}$ would be at a cost of 0.62 watt cm^{-3}.

Power loss including all radiation is plotted in Figs. 6 and 7. These data were obtained using calculated values of T_e, i.e., under the assumption that $-dN_e/dt = 0$,

and hence does not include any contribution from ion-electron pair production or loss. Comparing these results with corresponding Figs. 4 and 5, it is seen that the power loss in the first resonance line may be from one-half to two-thirds of the total radiative loss.

The results presented in Figs. 6 and 7 can be compared in a semi-quantitative fashion with those of Nighan,[7] who used a completely different approach in analyzing other experimental data of Reichelt.[8] The conditions of emitter temperature, cesium pressure and output current were similar, but the emitter-collector spacing of the experiment in Ref. 8 was 2 mm. Nighan calculated the rate of electron kinetic energy loss to the heavy particles due to both inelastic and elastic collisions, obtaining maximum values of 7.5 and 35 watt cm^{-3} at 4.0 and 8.5 amps cm^{-2}, respectively, independent of cesium pressure.

References

1. W. R. Reichelt, International Conference on Thermionic Electrical Power Generation, London, 1965.
2. D. W. Norcross and P. M. Stone, Report on Twenty-Sixth Annual Conference on Physical Electronics, Cambridge, Massachusetts, 1966.
3. P. M. Stone and D. W. Norcross, to be published.
4. L. Agnew, Proceedings of Thermionic Conversion Specialist Conference, San Diego, California, 1965.
5. T. Holstein, Phys. Rev. 83, 1159 (1951).
6. A. W. Ali and H. R. Griem, Phys. Rev. 140, A1044 (1965); Erratum, Phys. Rev. 144, A366 (1966).
7. W. L. Nighan, Proceedings of Thermionic Conversion Specialist Conference, Houston, Texas, 1966.
8. W. R. Reichelt and W. L. Kruer, Proceedings of Thermionic Conversion Specialist Conference, San Diego, California, 1965.

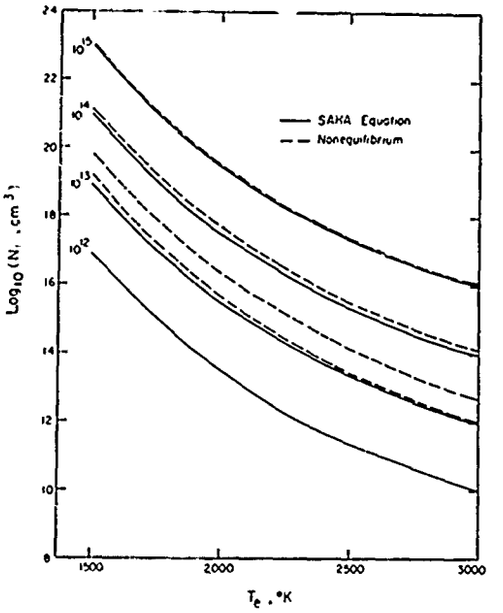

Fig. 1 Ground state density N_1 vs. electron temperature T_e for fixed N_e. Nonequilibrium ($\dot{N}_e = 0$) curves for same N_e values as Saha curves.

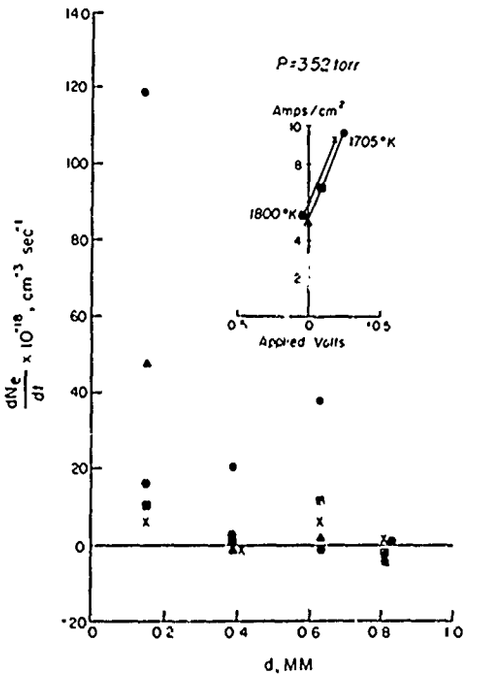

Fig. 2 Rate of electron-ion pair production calculated from the measured N_e, T_e profiles and the nonequilibrium model vs distance from the emitter. The collector is at 1.0 mm. The J-V curves are labeled with the emitter temperature.

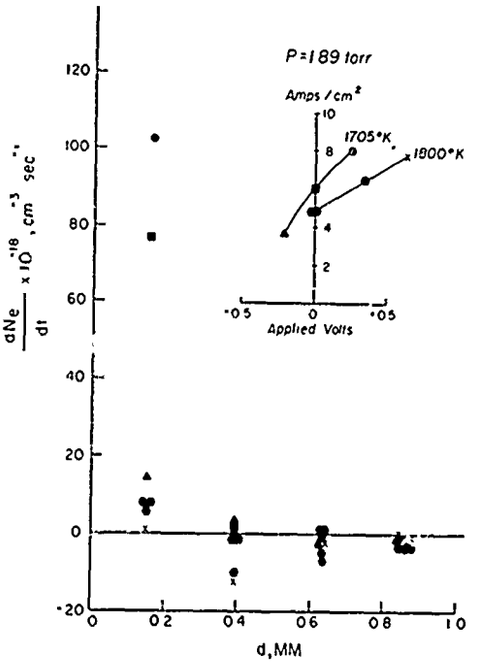

Fig. 3 Same as Fig. 2, but at a lower cesium pressure.

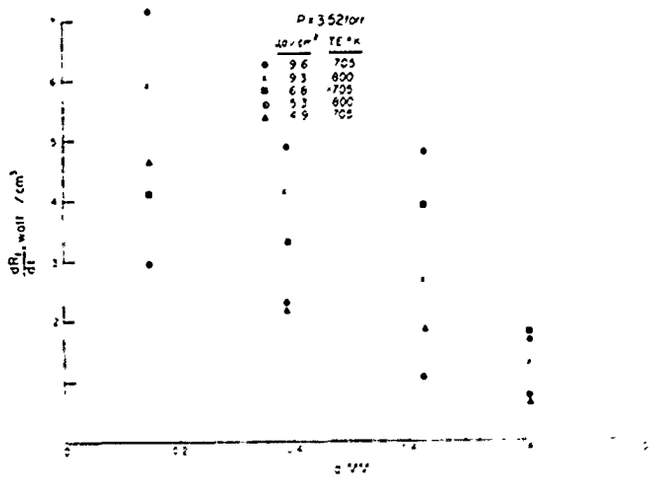

Fig. 4 Power loss from all sources except the resonance lines, calculated from the measured N_e, T_e profiles and the nonequilibrium model.

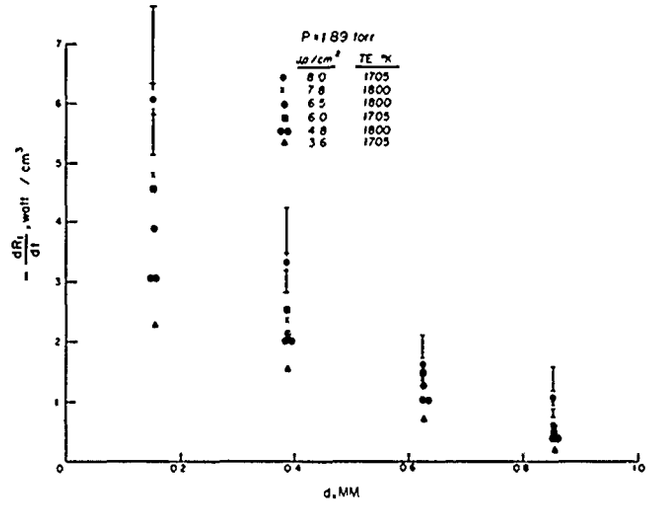

Fig. 5 Same as Fig. 4, but at a lower cesium pressure. The error bars indicate the effect of charges in T_e of 1% and 5%.

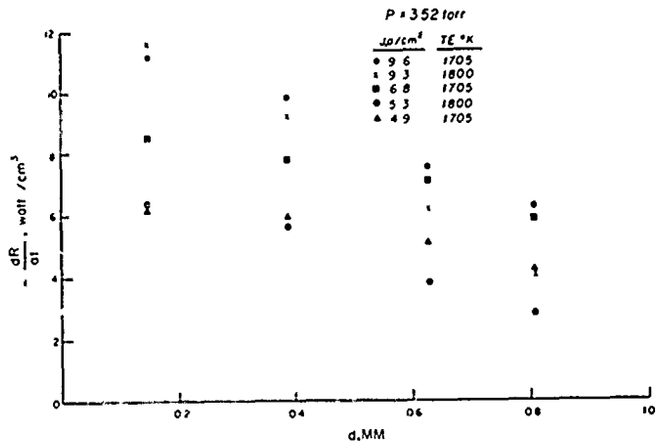

Fig. 6 Total radiative power loss calculated from the measured N_e profiles and the nonequilibrium model with $\dot{N}_e = 0$, $R = R_1 + R_3$.

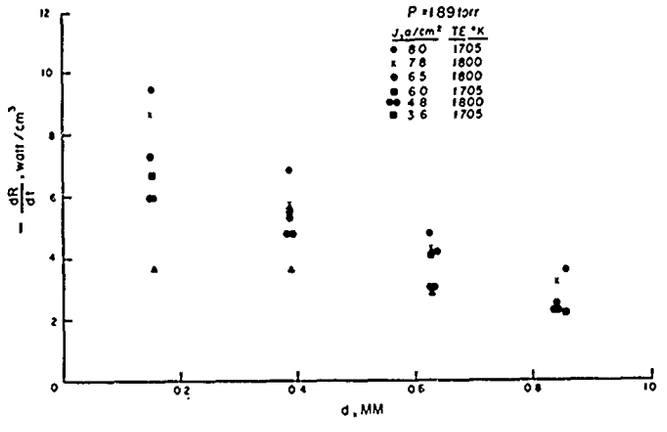

Fig. 7 Same as Fig. 6, but at a lower cesium pressure.

UNCLASSIFIED

Security Classification

DOCUMENT CONTROL DATA - R&D

(Security classification of title, body of abstract and indexing annotation must be entered when the overall report is classified)

1. ORIGINATING ACTIVITY (Corporate author) SPERRY RAND RESEARCH CENTER SUDBURY, MASSACHUSETTS 01776	2a. REPORT SECURITY CLASSIFICATION unclassified 2b. GROUP ---

3. REPORT TITLE

AN EXPERIMENTAL AND THEORETICAL STUDY OF THE NON-EQUILIBRIUM PLASMA IN THERMIONIC DISCHARGES

4. DESCRIPTIVE NOTES (Type of report and inclusive dates)

FINAL REPORT: 1 December 1966 - 30 November 1967

5. AUTHOR(S) (Last name, first name, initial)

Curry, Ronald H.; Norcross, David W.; Stone, Philip M.; Nygaard, Kaare J.

6. REPORT DATE	7a. TOTAL NO. OF PAGES	7b. NO. OF REFS
JANUARY 1968	66	51

8a. CONTRACT OR GRANT NO. Nonr-5154(00) b. PROJECT NO. NR 099-385 c. d.	9a. ORIGINATOR'S REPORT NUMBER(S) SRRC-CR-68-4 9b. OTHER REPORT NO(S) (Any other numbers that may be assigned this report)

10. AVAILABILITY/LIMITATION NOTICES

Reproduction in whole or in part is permitted for any purpose of the United States Government.

11. SUPPLEMENTARY NOTES Refer also to SRRC-CR-67-4, Annual Report No. 1 on Contract No. Nonr-5154(00).	12. SPONSORING MILITARY ACTIVITY Office of Naval Research Washington, D. C.

13. ABSTRACT Effective coefficients for ionization and radiative energy loss have been computed for different values of electron temperature and density. These coefficients and the neutral density yield the rates for net ion production and radiative energy loss from all sources except the resonance lines. Energy loss from resonance lines and the ion production cost are considered separately. The following general conclusions can be drawn: (1) the area within 0.4 mm of the emitter is a source of ion-electron pairs, the rest of the plasma being a sink; (2) inelastic energy losses decrease monotonically from the emitter to the collector; and (3) these effects are relatively independent of cesium pressure, but are generally proportional to output density. Furthermore, the differential equations governing the transport of particles, momentum, and energy in the plasma between the electrodes of a thermionic converter have been more completely formulated. Specific advances are the inclusion of more exact coefficients for electron transport and for ion production and radiative energy loss in the plasma volume.

In diode experiments, the electron temperature T_e was determined from measurement of the continuum emitted by radiative recombination to the 6P states of cesium, and the electron density N_e was determined from Stark broadening of the fundamental series lines. Spatial measurements of N_e and T_e were made. Of particular interest is observation of forbidden lines. The total ionization due to the passage of an electron beam in cesium vapor has been measured with a Tate and Smith apparatus, modified to include the retarding potential difference method. The cross section for production of Cs^+ ions has been determined from threshold to 100 eV. At threshold we found a slope of 2.7 $Å^2$/eV, as compared to the value 2.2 $Å^2$/eV determined by Heil and Scott.

DD FORM 1 JAN 64 1473

UNCLASSIFIED

Security Classification

UNCLASSIFIED

Security Classification

14. KEY WORDS	LINK A		LINK B		LINK C	
	ROLE	WT	ROLE	WT	ROLE	WT
Ion production Energy loss Electron temperature Electron density Transport equations Thermionic converter Cesium diode Plasma physics						

INSTRUCTIONS

1. ORIGINATING ACTIVITY: Enter the name and address of the contractor, subcontractor, grantee, Department of Defense activity or other organization *(corporate author)* issuing the report.

2*a*. REPORT SECURITY CLASSIFICATION: Enter the overall security classification of the report. Indicate whether "Restricted Data" is included. Marking is to be in accordance with appropriate security regulations.

2*b*. GROUP: Automatic downgrading is specified in DoD Directive 5200.10 and Armed Forces Industrial Manual. Enter the group number. Also, when applicable, show that optional markings have been used for Group 3 and Group 4 as authorized.

3. REPORT TITLE: Enter the complete report title in all capital letters. Titles in all cases should be unclassified. If a meaningful title cannot be selected without classification, show title classification in all capitals in parenthesis immediately following the title.

4. DESCRIPTIVE NOTES: If appropriate, enter the type of report, e.g., interim, progress, summary, annual, or final. Give the inclusive dates when a specific reporting period is covered.

5. AUTHOR(S): Enter the name(s) of author(s) as shown on or in the report. Enter last name, first name, middle initial. If military, show rank and branch of service. The name of the principal author is an absolute minimum requirement.

6. REPORT DATE: Enter the date of the report as day, month, year; or month, year. If more than one date appears on the report, use date of publication.

7*a*. TOTAL NUMBER OF PAGES: The total page count should follow normal pagination procedures, i.e., enter the number of pages containing information.

7*b*. NUMBER OF REFERENCES: Enter the total number of references cited in the report.

8*a*. CONTRACT OR GRANT NUMBER: If appropriate, enter the applicable number of the contract or grant under which the report was written.

8*b*, 8*c*, & 8*d*. PROJECT NUMBER: Enter the appropriate military department identification, such as project number, subproject number, system numbers, task number, etc.

9*a*. ORIGINATOR'S REPORT NUMBER(S): Enter the official report number by which the document will be identified and controlled by the originating activity. This number must be unique to this report.

9*b*. OTHER REPORT NUMBER(S): If the report has been assigned any other report numbers *(either by the originator or by the sponsor)*, also enter this number(s).

10. AVAILABILITY/LIMITATION NOTICES: Enter any limitations on further dissemination of the report, other than those imposed by security classification, using standard statements such as:

(1) "Qualified requesters may obtain copies of this report from DDC."

(2) "Foreign announcement and dissemination of this report by DDC is not authorized."

(3) "U. S. Government agencies may obtain copies of this report directly from DDC. Other qualified DDC users shall request through _____."

(4) "U. S. military agencies may obtain copies of this report directly from DDC. Other qualified users shall request through _____."

(5) "All distribution of this report is controlled. Qualified DDC users shall request through _____."

If the report has been furnished to the Office of Technical Services, Department of Commerce, for sale to the public, indicate this fact and enter the price, if known.

11. SUPPLEMENTARY NOTES: Use for additional explanatory notes.

12. SPONSORING MILITARY ACTIVITY: Enter the name of the departmental project office or laboratory sponsoring *(paying for)* the research and development. Include address.

13. ABSTRACT: Enter an abstract giving a brief and factual summary of the document indicative of the report, even though it may also appear elsewhere in the body of the technical report. If additional space is required, a continuation sheet shall be attached.

It is highly desirable that the abstract of classified reports be unclassified. Each paragraph of the abstract shall end with an indication of the military security classification of the information in the paragraph, represented as *(TS)*, *(S)*, *(C)*, or *(U)*.

There is no limitation on the length of the abstract. However, the suggested length is from 150 to 225 words.

14. KEY WORDS: Key words are technically meaningful terms or short phrases that characterize a report and may be used as index entries for cataloging the report. Key words must be selected so that no security classification is required. Identifiers, such as equipment model designation, trade name, military project code name, geographic location, may be used as key words but will be followed by an indication of technical context. The assignment of links, rules, and weights is optional.

GPO 886-551